The Role of "Vortical" Hot Towers in the Formation of Tropical Cyclone Diana (1984)

Eric A. Hendricks and Michael T. Montgomery

Department of Atmospheric Science, Colorado State University, Fort Collins, Colorado

Christopher A. Davis

National Center for Atmospheric Research, Boulder, Colorado

ABSTRACT

A high-resolution (3-km horizontal grid spacing) near-cloud-resolving numerical simulation of the formation of Hurricane Diana (1984) is used to examine the contribution of deep convective processes to tropical cyclone formation. This study is focused on the 3-km horizontal grid spacing simulation because this simulation was previously found to furnish an accurate forecast of the later stages of the observed storm life cycle. The numerical simulation reveals the presence of vortical hot towers, or cores of deep cumulonimbus convection possessing strong vertical vorticity, that arise from buoyancy-induced stretching of local absolute vertical vorticity in a vorticity-rich prehurricane environment.

At near-cloud-resolving scales, these vortical hot towers are the preferred mode of convection. They are demonstrated to be the most important influence to the formation of the tropical storm via a two-stage evolutionary process: (i) preconditioning of the local environment via diabatic production of multiple small-scale lower-tropospheric cyclonic potential vorticity (PV) anomalies, and (ii) multiple mergers and axisymmetrization of these low-level PV anomalies. The local warm-core formation and tangential momentum spinup are shown to be dominated by the organizational process of the diabatically generated PV anomalies; the former process being accomplished by the strong vertical vorticity in the hot tower cores, which effectively traps the latent heat from moist convection. In addition to the organizational process of the PV anomalies, the cyclogenesis is enhanced by the aggregate diabatic heating associated with the vortical hot towers, which produces a net influx of low-level mean angular momentum throughout the genesis.

Simpler models are examined to elucidate the underlying dynamics of tropical cyclogenesis in this case study. Using the Sawyer–Eliassen balanced vortex model to diagnose the macroscale evolution, the cyclogenesis of Diana is demonstrated to proceed in approximate gradient and hydrostatic balance at many instances, where local radial and vertical accelerations are small. Using a shallow water primitive equation model, a characteristic "moist" (diabatic) vortex merger in the cloud-resolving numerical simulation is captured in a large part by the barotropic model. Since a moist merger results in a stronger vortex and occurs twice as fast as a dry merger, it is inferred (consistent with related work) that a net low-level convergence can accelerate and intensify the merger process in the real atmosphere.

Although the findings reported herein are based on a sole case study and thus cannot yet be generalized, it is believed the results are sufficiently interesting to warrant further idealized simulations of this nature.

1. Introduction

Tropical cyclones form in the presence of mesoscale convective complexes in tropical disturbances (e.g., Gray 1968; Cotton and Anthes 1989). Cumulus convection is therefore believed to be an essential ingredient in the formation process. The pathway by which cumulus convection "organizes" to form a larger-scale tropical cyclone vortex is, to us, one of the great unsolved problems in dynamical and tropical meteorology.

Long ago, the role of cumulus convection was hypothesized to cooperate with the larger-scale vortex in a positive feedback process (Ooyama 1964; Charney and Eliassen 1964); this idea was later coined the conditional instability of the second kind, or "CISK." Contrary to this view, a wind-induced surface heat exchange process (WISHE) has been demonstrated to be the primary mechanism for tropical storm intensification (Ooyama 1969; Rotunno and Emanuel 1987), with cumulus convection transporting the ocean surface heat to the upper troposphere. As Montgomery and Farrell (1993) and others have pointed out, however, neither the CISK nor WISHE theories are appropriate descriptions of the tropical cyclogenesis process, since they implicitly assume that a transformation from a tropical disturbance to a finite amplitude surface concentrated rotary system

Corresponding author address: Dr. Michael T. Montgomery, Department of Atmospheric Science, Colorado State University, Fort Collins, CO 80523-1371.
E-mail: mtm@atmos.colostate.edu

has already taken place. The major unsolved problem in tropical cyclogenesis thus becomes one of understanding how a weak-amplitude tropical disturbance is transformed into a surface vortex of sufficient strength that can then amplify via the WISHE process.

Recent studies have suggested that mesoscale convective vortices (MCVs), which form in the stratiform precipitation region at midlevels of the troposphere in disturbed weather regions, are a precursor to tropical cyclogenesis (Bister and Emanuel 1997, hereafter BE97; Ritchie and Holland 1997, hereafter RH97). Both of these studies suggest that midlevel MCVs are necessary for building a surface vortex: BE97 hypothesized that vertical vorticity was advected downward via mesoscale subsidence in association with stratiform precipitation, while RH97 advocated the idea of downward development by a succession of midlevel mergers between MCVs that form in the stratiform precipitation region *following* deep convective episodes. Both of these theories are regarded here as "top down" mechanisms for the development of the necessary seedling vortex at the ocean surface. Recent work (Montgomery and Enagonio 1998, hereafter ME98) has suggested an altogether different mechanism for the development of the surface vortex.

In mesoscale convective systems associated with easterly waves or extratropical troughs, small-scale cores of towering cumulonimbus convection, or hot towers, are frequently observed to exist. While past work has analyzed the role of hot towers in the vertical heat transport and mass flux of the tropical overturning circulation (Hadley cell; Riehl and Malkus 1958, hereafter RM58), little work has been devoted to examining the dynamical role that these structures may play in incipient hurricane formation. Simpson et al. (1998) put forth the idea that the hot towers were a positive influence to genesis via subsidence warming around them and the attendant surface pressure falls. In a different light, ME98 and Möller and Montgomery (2000) demonstrated that low-level vortex merger and axisymmetrization of small-scale diabatically generated cyclonic potential vorticity (PV) anomalies (from hot-tower-like "convective bursts") could intensify a larger-scale vortex on realistic time scales.

Observations have generally been inadequate to fully capture the tropical cyclogenesis process because tropical cyclones typically form in the deep Tropics far away from landmasses. In fact, only a few observational experiments of genesis have been conducted to date, namely, the Tropical Experiment in Mexico (TEXMEX; BE97) and the Tropical Cyclone Motion experiments (TCM-92; RH97). With recent advances in computer technology, the formation of incipient hurricanes can now be studied using powerful mesoscale numerical models that provide the solution to the primitive equations at very high resolution (less than 10 km in horizontal gridpoint spacing). One such model simulation captured the formation of Hurricane Diana (1984; Davis

and Bosart 2001, hereafter DB01) with 9-km horizontal grid spacing. Using this simulation, DB01 studied the transformation of the initial subtropical disturbance into a tropical storm with accurate intensification timing in comparison to the observations.

Hurricane Diana formed in a modest baroclinic environment just east of Florida in September 1984. It falls into the class of tropical cyclones that form in subtropical, baroclinic environments often with forced ascent from one or more upper-level cyclonic potential vorticity anomalies. Diana was a useful case to study since it formed close to land and had a good observational network. Bosart and Bartlo (1991, hereafter BB91) provided a comprehensive observational analysis of the formation process based on available data. They concluded that the upper-level potential vorticity anomaly left after a "trough fracture" was essential to stimulating the genesis of the storm (see Montgomery and Farrell 1993 and DB01 for more details).

In the present study we undertake an analysis of the role of hot towers possessing strong vertical vorticity in their cores, or "vortical" hot towers, in the formation of Hurricane Diana using a high-resolution (3-km horizontal grid spacing) near-cloud-resolving numerical simulation with the fifth-generation Pennsylvania State University–National Center for Atmospheric Research (PSU–NCAR) Mesoscale Model (MM5). To the authors' knowledge, this is the first study conducted examining vortical hot towers and their collective effect in this framework.

The vortical hot towers are found to be the preferred mode of convection at near-cloud-resolving scales. We will demonstrate that they are the most important ingredients for forming the incipient tropical storm via a two-stage process: (i) preconditioning of the local environment via diabatic production of multiple small-scale lower-tropospheric cyclonic PV anomalies, and (ii) multiple mergers and axisymmetrization of these low-level PV anomalies. The warm-core formation and tangential momentum spin-up will be shown to be ultimately the result of the organizational process of the diabatically generated PV anomalies; the foregoing process being accomplished by the strong vorticity in the anomaly cores, which tends to trap the latent heat from moist convection. We will demonstrate that simpler models broadly capture the key vortical/convective processes in the explicit cloud numerical simulation. Using the Eliassen-balanced vortex model (Eliassen 1951), many key stages of the organization of Diana will be shown to proceed in quasi balance. Additionally, the diabatic heating associated with the vortical hot towers will be shown to force a mean mesoscale secondary circulation that produces a net low-level influx of mean angular momentum and increased low-level ambient vertical vorticity. Using the shallow water primitive equation model the role of "moist" processes in vortex merger is clarified.

The outline of this paper is as follows. In section 2,

the mesoscale model used for the numerical simulation is described. The numerically simulated vortical hot towers are analyzed in section 3. Local tangential momentum and heat budgets are analyzed for characteristic events in section 4. In section 5, the quasi-balanced dynamics of the cyclogenesis process is assessed. A comparison of the moist and dry dynamics of vortex merger is discussed in section 6. A summary of the important findings in this study and recommendation for future work are presented in section 7.

2. Description of 3-km numerical experiment

The PSU–NCAR MM5 version 2.0 is used for the numerical simulation (Grell et al. 1995). The model used here is nonhydrostatic and formulated in terrain-following σ coordinates. Briefly, the prognostic equations are for horizontal and vertical momentum, pressure, temperature, water vapor, cloud water, and rainwater. The following schemes are used to represent subgrid-scale atmospheric physical processes: the medium-range forecast (MRF) planetary boundary layer (PBL) scheme (Hong and Pan 1996), the numerical weather prediction explicit microphysics scheme (NEM; Schultz 1995), and the Dudhia (1989) radiation scheme. In the 3-km simulation described in this manuscript, cumulus convection is calculated explicity at the grid scale. [In the 9-km simulation in DB01, the Kain–Fritsch cumulus scheme (Kain and Fritsch 1990) was employed.] More detail on the MM5 and these schemes can be found in Dudhia (1993) and Grell et al. (1995). The predictive equations are integrated with a standard leapfrog time stepping combined with an Asselin filter.

For this simulation, the model configuration consists of four nested domains of horizontal grid spacing 81 km (domain 1), 27 km (domain 2), 9 km (domain 3), and 3 km (domain 4; Davis and Bosart 2002, hereafter DB02). A diagram of these four domains and their corresponding locations can be found in Fig. 1. The model is initialized on 1200 UTC 7 September 1984, corresponding to $t = 0$ h, and the 3-km domain is inserted at $t = 21$ h (DB02). At the initialization time, the actual tropical cyclone (TC) Diana had not formed and is a subtropical disturbance. This simulation is therefore considered very useful for understanding tropical cyclogenesis since it captures the transition from a baroclinic-type disturbance to a warm-core tropical storm.

The model is initialized using the National Centers for Environmental Prediction (NCEP)–NCAR reanalysis data and with dynamically balanced initial conditions. There is no bogus vortex used in the model. The coarser resolution domains of 81 and 27 km capture the synoptic-scale forcing responsible for stimulating the cumulus convection on the mesoscale; the highest 3-km resolution domain captures the small-scale dynamics of the organizational process of the incipient tropical storm, which is the main focus of this paper.
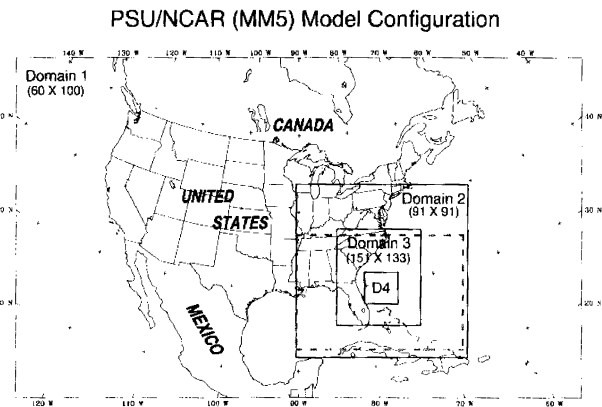
A description of the 3-km grid is as follows. The

FIG. 1. The configuration of the PSU–NCAR MM5 for the simulations of the genesis of TC Diana (from DB01). All four nested domains are shown with their relative location to the United States. The 3-km domain is domain 4 (D4) and it is fixed in the same location for the genesis phase studied here.

domain consists of 146 by 146 horizontal grid points, for a total domain size of 438 km by 438 km. There are initially 37 vertical terrain-following model levels between the surface and the 50-hPa pressure level. These levels are staggered such that better resolution exists at lower levels. For computational ease and to minimize data storage, we interpolate the model output data to a new vertical grid of 19 levels with equidistant spacing of $\delta z \approx 600$ m. The 3-km domain is held fixed in the same global position (just off the east coast of Florida) during the genesis phase studied here, and the location is chosen since it captures the entire tropical storm genesis during the time period.

From the simulation executed in DB01 (which had a highest resolution of 9-km horizontal grid spacing), the following is a summary of the simulated phases of genesis. From $t = 0$ h to $t = 24$ h there exists a disturbance with no closed surface low pressure. From $t = 24$ h to $t = 36$ h a weak surface low develops (i.e., Diana becomes a tropical depression) and by $t = 36$ h Diana has attained tropical storm strength. Also, during this time period there are numerous asymmetries in cumulus convection. These asymmetries, or "eddies," were shown by DB01 to be essential to the storm-relative tangential momentum budget in the 9-km simulation, shown in Fig. 2. Motivated by the work of DB01 using a 9-km grid, we look here to gain a more detailed understanding of the role of these convective asymmetries with the higher-resolution cloud-resolving simulation of 3-km gridpoint spacing.

3. Simulated vortical hot towers

Before analyzing the simulated convection in the cloud-resolving numerical simulation, it proves informative to illustrate hot towers in an observed developing tropical storm. In Fig. 3, the *Geostationary Operational Environmental Satellite-8* (*GOES-8*) visible satellite im-
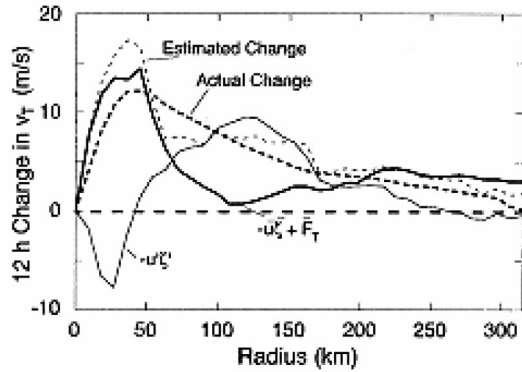
FIG. 2. Integrated tangential momentum budget from $t = 23$ h to $t = 34$ h in the 9-km horizontal grid spacing experiment executed by DBO1. The horizontal eddy vorticity flux is shown to be crucial to spinup between $r = 50$ km and $r = 200$ km.

agery of Tropical Storm Gustav (2002) is shown at two different ranges on 1925 UTC 9 September 2002. The top panel presents a larger-scale perspective and the bottom panel presents a close-up view. Since Gustav was heavily sheared from the northeast, the visible satellite imagery provides us with the unique opportunity to see the overshooting cirrus canopies of the deep convection as well as the low-level mesovortices. Since there is no orographic forcing from nearby islands and since the scale of the low-level mesovortices is approximately the same as the convective blowups, it stands to reason that these low-level intense mesovortices must have originated from the deep convection and accompanying low-level convergence of relative vorticity from the vorticity-rich environment of the larger-scale vortex circulation. The importance of the mesovortices in this tropical storm development is believed to lie in the axisymmetrization of the low-level anomalies into the larger-scale vortex (ME98).

In the numerical simulation studied here, the hot towers will be shown to be robust and persistent structures. Convection formed in the pre-Diana disturbance due to favorable environmental conditions (BB91 and DB01), including significant convective available potential energy (CAPE). CAPE is calculated using the model output data based on pseudoadiabatic ascent. As an example of this, the model-calculated surface-based CAPE at $t = 26.2$ h is shown in Fig. 4. In the region of the convection, CAPE values are approximately 1500 to 2500 J kg^{-1}. It is reasonable to assume that these hot towers formed in the most unstable areas of the environment. We now examine the simulated hot towers in detail.

a. Scale, intensity, and vertical structure

The simulated deep convection is identified in the model output by variables that would be typically expected in deep cumulus convection: positive vertical velocity (w), positive diabatic heating rate ($\dot{\theta}$), and the existence of hydrometeors (diagnosed here simply by the model variable of liquid water content, or w_l). The diabatic heating rate $\dot{\theta}$ is calculated by residual of the θ field in space and time; that is $\dot{\theta} = \partial\theta/\partial t + \mathbf{v} \cdot \nabla\theta$, where $\mathbf{v}$ is the three-dimensional velocity vector. The characteristic structure of the deep convection is shown in Fig. 5. Here, plan views of vertical velocity and diabatic heating rates are shown with the associated vertical profile of the field in the core. The horizontal scale of the hot tower here is approximately 10 km; measured by the diameter of the $w = 3.0$ m s^{-1} contour at midlevels. In this characteristic hot tower, the peak core vertical velocity is 15 m s^{-1} and the peak diabatic heating rate is 150 K h^{-1} at midlevels ($z \approx 5$ km) of the troposphere. The vertical structure of the vertical velocity and diabatic heating rate indicates that towering cumulonimbus convection is being simulated.

All the hot towers at $t = 26.2$ h and at other times have been examined in a similar manner. A representative statistical summary of these hot towers at $t = 26.2$ h can be found in Table 1. This time is chosen since numerous hot towers are appearing and Diana is still just a disturbance. The hot towers are generally confined to a horizontal scale of approximately 10 km (by the same criterion used in defining the example hot tower) and are characterized by, on average, peak core vertical velocities of 9 m s^{-1} and peak core diabatic heating rates of 150 K h^{-1} at midlevels of the troposphere. At a later time, $t = 30$ h, when Diana is a tropical depression, the hot towers are examined and similar results are found. At this time the average peak core vertical velocity is 8.8 m s^{-1} and the average peak diabatic heating rate is also 150 K h^{-1}.

A higher-resolution simulation of the genesis of Hurricane Diana has been performed by the third author [in collaboration with Jordan Powers of the NCAR Mesoscale and Microscale Meteorology (MMM) group] with 1.2-km horizontal grid spacing (Powers and Davis 2002). Preliminary examination of these data indicates that the 1.2-km convection is quite similar to the 3-km convection in intensity, that is, the maximum updrafts are approximately 10 m s^{-1} in the cores of the hot towers at midlevels. The scale of the 1.2-km hot towers is somewhat smaller. Typical hot towers are approximately 5–7 km in diameter in this experiment, in comparison to the 10-km diameter hot towers in the 3-km experiment. Although an analysis of the 1.2-km simulation results will be presented in a forthcoming publication, the fact that similar convective structures are observed in each simulation (1.2 and 3 km) leads us to believe that the 3-km simulation is at a resolution where these plumelike structures are becoming adequately simulated by the model. Additionally, Powers and Davis (2002) find that the mesoscale essentials of the storm's development are captured at the 3-km resolution. As we will soon see, the phenomenology of these vortical plumes appears similar in some respects to recent findings in studies of rapidly rotating Rayleigh–Benard convection (Julien et
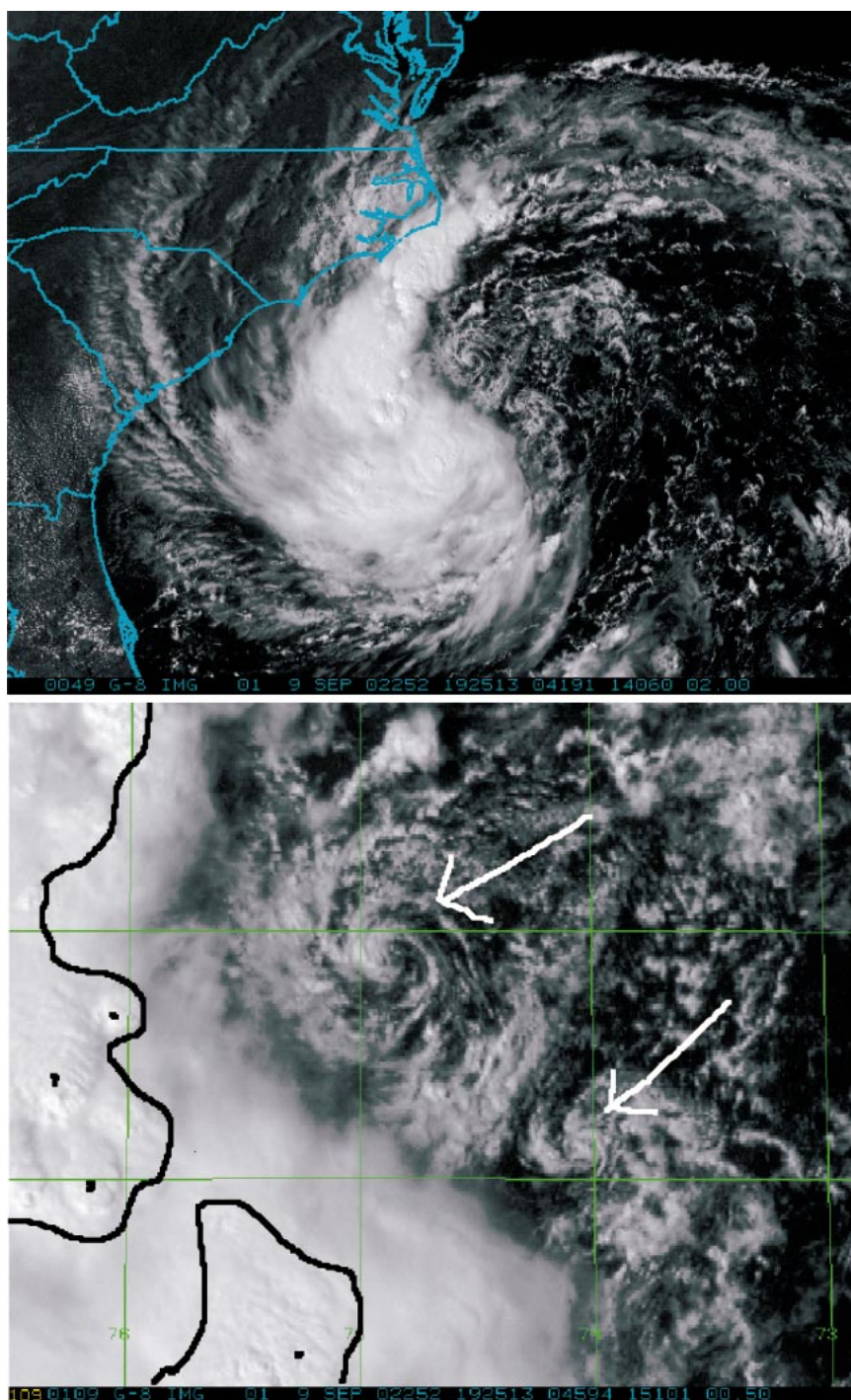
FIG. 3. *GOES-8* visible satellite images of Tropical Storm Gustav (2002) at 1925 UTC 9 Sep 2002. (top) A larger-scale perspective; (bottom) a close-up view, where the region of deep convection is marked by the black line, and some individual hot towers are marked by black dots. Low-level exposed mesovortices are identified by the white arrows. Images are courtesy of Mark DeMaria and Raymond Zehr of NOAA/NESDIS/CIRA Fort Collins, CO.
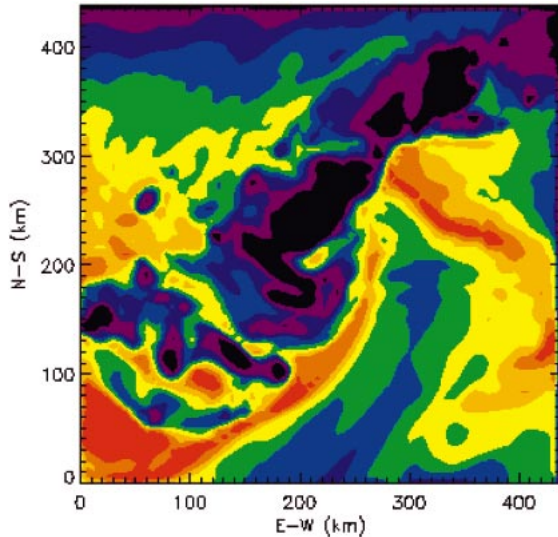
FIG. 4. MM5-calculated surface-based CAPE at $t = 26.2$ h for the entire 3-km domain. Contour intervals are as follows: 0–300 J kg^{-1} (black), 300–600 J kg^{-1} (purple), 600–900 J kg^{-1} (dark blue), 900–1200 J kg^{-1} (light blue), 1200–1500 J kg^{-1} (green), 1500–1800 J kg^{-1} (yellow), 1800–2100 J kg^{-1} (orange), 2100–2400 J kg^{-1} (dark orange), and 2400 J kg^{-1} and above (red).

al. 1996; Legg et al. 2001; Julien et al. 1999). On the basis of these considerations, the 3-km simulation is believed to be an adequate estimate of the moist convective/vortex dynamics and we will use these data to develop the basic conceptual model of tropical cyclone Diana's organizational process.

b. Lower-tropospheric cyclonic PV towers

As stated earlier, these hot towers are unlike typical tropical hot towers (e.g., those described in RM58). These hot towers possess intense vorticity in their cores. This vorticity is expected to inhibit lateral entrainment (Julien et al. 1996; Helfrich 1994; Ayotte and Fernando 1994) thereby making the convection more efficient. As an example of the vortical and rotational aspects of the hot towers simulated here, the low-level horizontal wind vectors associated with a hot tower at $t = 23.5$ h are shown in Fig. 6. We see that there is a closed circulation around the hot tower of an approximate scale of 10 to 20 km, and strong tangential winds around the tower exists; on the north side of the vortex, winds are approximately 15–20 m s^{-1} and on the south side winds are approximately 5–10 m s^{-1}.

In this section, we examine how the hot towers modify the existing potential vorticity field. This is important since hurricanes ultimately are characterized by strong PV in their cores, and for genesis it is central to understand how this PV (and vorticity) is created and assembled. We first recall the prognostic PV equation in material form (e.g., Holton 1992):

$$\frac{D(\text{PV})}{Dt} = \frac{\zeta_a}{\rho} \cdot \nabla \dot{\theta} + \frac{1}{\rho}(\nabla \times \mathbf{F}) \cdot \nabla \theta. \qquad (1)$$

Here, ζ_a is the absolute vorticity vector and $\mathbf{F}$ is the friction vector, which includes all turbulent processes that cannot be resolved by the prognostic state variables for the given grid scale. As shown by Eq. (1), the nonconservation of PV is dictated by local sources or sinks of diabatic heating and friction. In hot towers, where diabatic heating rates are very strong, internal friction can be neglected in comparison. The PV equation can be further reduced since above the boundary layer horizontal vorticity is found to be at least an order of magnitude less than the vertical vorticity in the hot tower cores. The simplified PV equation is then,

$$\frac{D(\text{PV})}{Dt} \approx \frac{f + \zeta}{\rho} \frac{\partial \dot{\theta}}{\partial z}. \qquad (2)$$

This approximate PV equation is useful since it indicates that the nonconservation of PV is controlled principally by the vertical gradient of diabatic heating in the hot towers (ME98). For the representative hot towers shown in Fig. 5, the vertical gradient of the diabatic heating rate is generally positive from the surface to $z \approx 5$ km and negative above $z \approx 5$ km. Moreover, the gradient ($\partial \dot{\theta}/\partial z$) is nearly constant and large in absolute value in both of these regions. For example, in the region between $z = 0$ to $z = 5$ km, $|\partial \dot{\theta}/\partial z| \approx 45$ K h^{-1} km^{-1}. Substituting this value into the PV equation in conjunction with lower-tropospheric layer-averaged values of density and vorticity in the hot towers, a rough estimate of the lower-tropospheric production rate inside the hot tower cores can be determined:

$$\frac{D(\text{PV})}{Dt} \approx \frac{10^{-3} \text{ s}^{-1}}{0.7 \text{ kg m}^{-3}}(1.25 \times 10^{-5} \text{ K s}^{-1} \text{ m}^{-1})$$
$$\approx 64 \text{ PVU h}^{-1}, \qquad (3)$$

where 1 PVU $= 1 \times 10^{-6}$ m^2 s^{-1} K kg^{-1} (Hoskins et al. 1985).

A typical hot tower in this simulation will be producing lower-tropospheric PV at a peak material rate of $+64$ PVU h^{-1} in its core from $z = 0$ to $z = 5$ km, and diminishing PV above that by approximately the same rate. In summary, the net effect of the hot towers is to produce strong small-scale (10 km in diameter on average) lower-tropospheric (below $z \approx 5$ km) cyclonic PV towers. From a vorticity dynamics perspective, the strong updrafts in the hot towers converge and stretch existing low-level vertical vorticity into intense small-scale vortex tubes (e.g., Fig. 3).

4. Local tangential momentum and heat budgets

The 3-km cloud-resolving numerical simulation reveals a two-phase evolution characterized by the organizational process of the hot towers. The first phase is a preconditioning phase in which the hot towers are
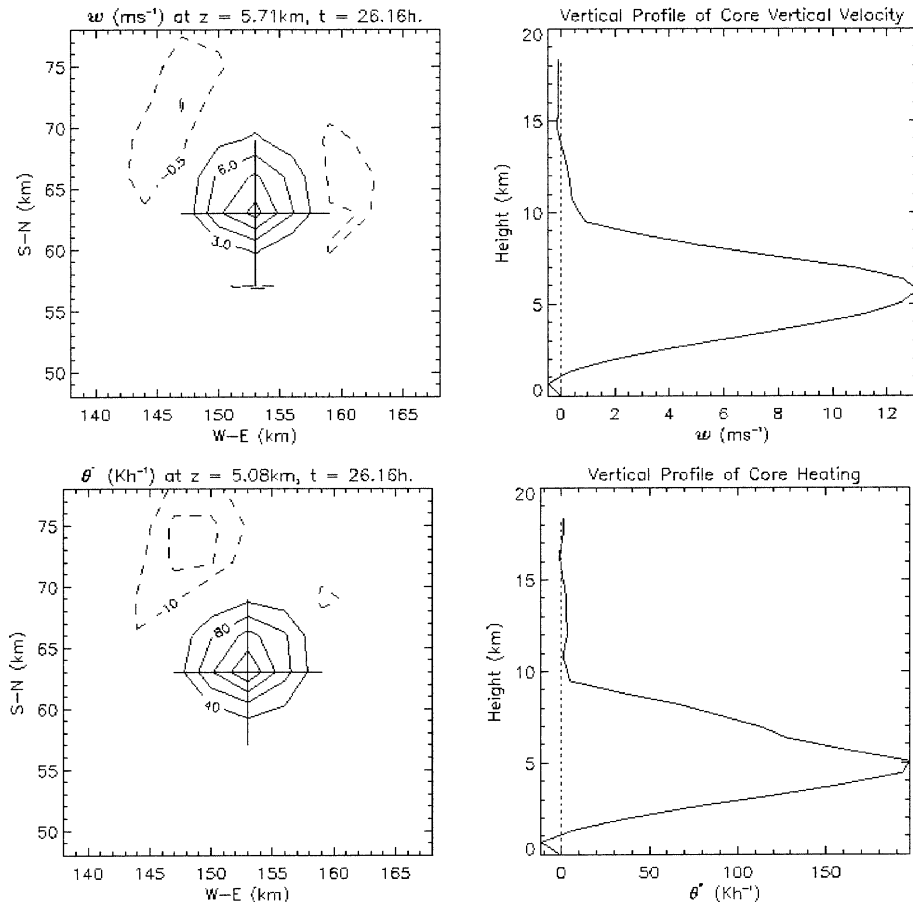
FIG. 5. Characteristic vertical structure of simulated hot towers. (left) Plan views of the hot tower (top) vertical velocity and (bottom) diabatic heating rate at midlevels. (right) Vertical profiles of the hot tower (top) vertical velocity and (bottom) diabatic heating rate at the point marked by the cross in the left panels.

pulsing and locally enhancing lower-tropospheric PV and vorticity, thereby increasing the likelihood of tropical cyclogenesis (cf. Ooyama 1982). The second phase is characterized by multiple mergers/axisymmetrization of these PV or vorticity anomalies. For the simulation studied here, the preconditioning phase lasts from $t = 21$ h to $t \approx 27$ h and the multiple vortex merger phase lasts from $t \approx 27$ h to $t = 36$ h.

We now examine tangential momentum and heat budgets in characteristic "events" during each phase in order to obtain a more quantitative understanding of the dynamics of tangential momentum spinup or spindown and warm- or cold-core tendencies.

Since there is no well-defined center during the genesis period being studied here, budgets are examined during specific events that appear important to the genesis of the storm. These events are interactions of PV anomalies generated by the hot towers, or events where amalgamations or potential mergers occur. Since the horizontal scale of a tropical cyclone is typically much larger than the hot tower scale, these interactions are believed central to our hypothesis that TC Diana (as

simulated here) is in essence "built" by the vortical hot towers. When an event is identified to be of interest, a fixed center is chosen at the center of the resultant anomaly created by the amalgamation process; this center is also the approximate PV centroid of the event in question. All variables are then remapped into a cylindrical coordinate system about this local center, and then decomposed into a basic state (azimuthal mean) value plus a perturbation (eddy) value. To wit: given a variable A, we write

$$\overset{\text{total}}{\overbrace{A(r, \lambda, z, t)}} = \overset{\text{azimuthal mean}}{\overbrace{\overline{A}(r, z, t)}} + \overset{\text{perturbation}}{\overbrace{A'(r, \lambda, z, t)}}, \quad (4)$$

where

$$\overline{A}(r, z, t) = \frac{1}{2\pi} \int_0^{2\pi} A(r, \lambda, z, t) \, d\lambda. \quad (5)$$

The above integral is discretized into 50 azimuthal points at each radius (chosen to retain good horizontal resolution near the event center), and is computed in the following manner:

TABLE 1. Statistical summary of hot tower intensity at $t = 26.2$ h.

Hot tower no.	Peak updraft (m s^{-1})	Vertical level (km)	Peak heating (K h^{-1})	Vertical level (km)
1	13.0	5.71	195	5.08
2	9.5	8.86	112	8.23
3	6.7	6.97	153	6.34
4	9.2	6.34	92	6.34
5	5.7	4.45	85	3.19
6	16.3	8.23	250	6.97
7	15.0	6.97	205	5.71
8	10.2	4.45	201	4.45
9	9.2	4.45	185	4.45
10	9.2	6.34	128	5.08
11	4.2	7.60	175	6.97
12	9.0	6.97	163	5.08
13	8.6	6.97	192	5.08
14	10.5	6.34	98	7.60
15	9.5	5.71	182	5.71
16	7.6	8.23	263	5.71
17	9.6	7.60	101	6.34
18	13.0	6.34	72	8.23
19	6.5	5.71	68	6.34
20	4.7	8.86	101	6.34
21	7.0	6.34	171	6.34
22	7.3	6.34	143	6.34
23	12.2	7.60	101	6.34
Mean	9.3	6.67	149	6.01
Std dev	3.1	1.27	56	1.20

$$\overline{A}(r, z, t) = \frac{1}{50} \sum_{j=0}^{49} A(r, \lambda_j, z, t). \qquad (6)$$

Here, r is the radius from an arbitrary event center, z is the height, and λ is the azimuthal angle in radians. In this local cylindrical coordinate system, the budgets are analyzed by the decomposed formulation of the tangential momentum equation and thermodynamic equation. The equations are shown below in integral form, integrated from arbitrary times t_a to t_b, which encompass the event being examined. The mean integral tangential momentum balance (cf. Raymond et al. 1998) is then

$$\overline{v}(t_b) - \overline{v}(t_a)$$
$$= -\int_{t_a}^{t_b} (\overline{u}\;\overline{\eta})\, dt - \int_{t_a}^{t_b} \left(\overline{w}\frac{\partial \overline{v}}{\partial z}\right) dt - \int_{t_a}^{t_b} (\overline{u'\zeta'})\, dt$$
$$- \int_{t_a}^{t_b} \left(\overline{w'\frac{\partial v'}{\partial z}}\right) dt + \int_{t_a}^{t_b} (\overline{PBL} + \overline{DIFF})\, dt, \quad (7)$$

and the mean integral heat budget equation is, similarly,

$$\overline{\theta}(t_b) - \overline{\theta}(t_a)$$
$$= -\int_{t_a}^{t_b} \left(\overline{u}\frac{\partial \overline{\theta}}{\partial r}\right) dt - \int_{t_a}^{t_b} \left(\overline{w}\frac{\partial \overline{\theta}}{\partial z}\right) dt - \int_{t_a}^{t_b} \left(\overline{u'\frac{\partial \theta'}{\partial r}}\right) dt$$
$$- \int_{t_a}^{t_b} \left(\overline{w'\frac{\partial \theta'}{\partial z}}\right) dt + \int_{t_a}^{t_b} (\overline{\dot{\theta}})\, dt. \qquad (8)$$

The variables in the above equations are as follows: ζ is the relative vertical vorticity, η is the absolute ver-

tical vorticity $(f + \zeta)$, w is the vertical velocity, v is the tangential velocity, u is the radial velocity, θ is the potential temperature, PBL is the model planetary boundary layer subgrid-scale scheme, and DIFF is the model horizontal diffusion. The mean variables in each equation above are functions of r and z, as well as time.

The actual spinup (spindown) or warming (cooling) is recorded by the difference on the left-hand side of each equation, respectively, and the dynamics of that tendency is diagnosed by examining each term on the right-hand side. The estimated, or predicted, change is the summation of all the terms of the right-hand side. This estimated change must be well-correlated to the left-hand side in order to validate the diagnosed dynamics. Two representative budgets are now examined and they are described below.

a. Budget A: Example of "preconditioning"

A local budget representative of the preconditioning phase is presented here. The event chosen occurs where some vorticity anomalies appear to merge together into a larger-scale anomaly. A center is fixed at the location of the resultant low-level vorticity anomaly, and budgets are performed for the 3-h period prior to the formation of the resultant anomaly. Plan views of absolute vertical vorticity during this event are shown in Fig. 7, at $t = 23$ h, $t = 24$ h, and $t = 25$ h, at two model levels ($z = 0.67$ km and $z = 5.08$ km). There are some noteworthy features worth mentioning in this figure. The surface frontal boundary vorticity is denoted by the green strip in the southeastern portion of the domain. The strong vorticity anomalies associated with the hot towers are north of the surface front (shown by the red color), and they are advected to the southwest by the local flow. This phase is a preconditioning phase since the hot towers are creating strong vorticity anomalies in the lower troposphere, and creating a more favorable environment for hurricane formation. By $t = 25$ h, the initial frontal boundary vorticity is being swept into a strong hot tower, and the figure suggests strongly that the hot towers are controlling the evolution at this stage. Strong vorticity anomalies at mid- and low levels can be seen at each time in the figure. At $t = 24$ h, two strong vorticity anomalies can be seen, with $\eta \approx 30 \times 10^{-4}$ s^{-1}. By $t = 25$ h, there appears to be a merger of these anomalies at low levels.

The results of the azimuthal mean tangential momentum and heat budgets are shown in Figs. 8 and 9, respectively. In Fig. 8, only the dominant terms in the mean tangential momentum budget are displayed; these are the symmetric radial vorticity flux $-\overline{u}\overline{\eta}$ and the eddy radial vorticity flux $-\overline{u'\zeta'}$. In Fig. 8a it can be seen that there is a strong symmetric spinup tendency in this 3-h period, over 45 m s^{-1} in the core at low to middle levels. However, the eddies are causing a strong spindown at low levels, over -30 m s^{-1} in the same region. During this 3-h period, a net spinup of 5–10 m s^{-1} occurs
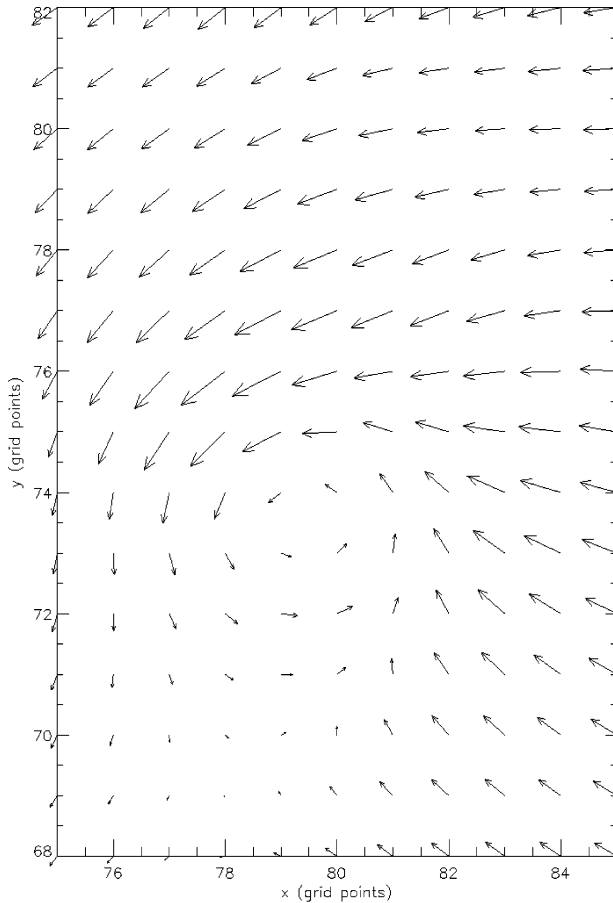
FIG. 6. The low-level wind vectors associated with a typical vortical hot tower at $t = 23.5$ h and $z = 0.67$ km. Axis values are grid points in the south–north (vertical) and west–east (horizontal) directions, with each grid point corresponding to a distance of 3 km. The small-scale vortex associated with the hot tower is evident in the wind vector field. The maximum winds on the north side of the hot tower are approximately 18 m s^{-1} and the maximum winds on the south side are approximately 8 m s^{-1}.

at low levels, mainly in response to the symmetric convergence of relative angular momentum. The sensitivity of the results to slightly moving the event center has been examined and it is found that the results do not change significantly; that is, the eddy term generally opposes the mean (spinup) term during this phase.

To fix ideas, in the bottom left of Fig. 7 there appears to be a vortex merger at low levels, as a vorticity anomaly appears to be axisymmetrized into the parent anomaly, marked by the white cross. Whether a vortex merger actually occurs, however, can be quantified clearly. Recalling simple vortex merger theory (Melander et al. 1988), a vortex merger is marked by a positive contribution from the radial eddy vorticity flux terms (i.e., $-\overline{u'\zeta'} \geq 0$). Examining the azimuthal mean eddy flux contribution (Fig. 8b), we see that there are multiple tropospheric regions where merger and nonmerger occur. The symmetric and eddy fluxes of vorticity tend to be nearly equal and opposite in these regions as well.

These results indicate that in this phase the vortex tubes generated by the hot towers are not cooperating in strong vortex mergers, but rather competing with one another to sustain themselves. Although these hot towers and associated vortex tubes are competing with one another, they act to increase the ambient lower-tropospheric relative vorticity in the region, and therefore serve to "precondition" the atmosphere for storm formation at a later time (cf. Ooyama 1982).

Examining the heat budget for this event (Fig. 9b), we see that local warming occurs in the vicinity of the hot towers, approximately 2–3 K at low to middle levels. However, this warming is confined to a local area $r \leq 10$ km from the event center. The estimated and actual change agree well qualitatively and quantitatively, shown in Figs. 9a and 9b. The two dominant terms in the heat budget are the mean diabatic heating rate tendency $(\overline{\dot{\theta}})$ and the mean vertical heat advection $-(\overline{w}\partial\overline{\theta}/\partial z)$, as shown in Figs. 9c and 9d, respectively. Examining Fig. 9d, we see that subsidence warming is not responsible for the core warming that occurs in this event; that is, $-\overline{w}\partial\overline{\theta}/\partial z$ is generally negative in the entire troposphere. Rather, in the convecting region there is rising motion and adiabatic cooling of air parcels, and the warming that occurs is due mainly to the residual in the diabatic heating and adiabatic cooling in the convection that tends to become trapped there due to high vorticity in the central regions (e.g., Hack and Schubert 1986). The results in Fig. 9 suggest that the heat is being trapped in the vicinity of the vortical hot towers.

b. Budget B: Example of "diabatic vortex merger"

The second phase of genesis is characterized by multiple mergers of convectively generated PV or vorticity anomalies from the hot towers. Three examples of these mergers are shown in Fig. 10 (and an animation of this phase can be found online at http://eliassen.atmos. colostate.edu/eric.html). A noteworthy merger event occurs near $t = 34$ h, where two intense vorticity anomalies merge together. As a result of this event, the seedling tropical storm vortex is born. This event is depicted in three stages in Fig. 11. Here the axisymmetrization (i.e., the decay of the asymmetries in favor of creating a master vortex) of these two lower-tropospheric vortex tubes is clearly evident. The merger here occurs more strongly at low levels. The dominant contributions to the tangential momentum and heat budgets are examined during this event; these are shown in Figs. 12 and 13, respectively.

As shown by Fig. 12d, a broad area of low-level spinup occurs during this event, peaking at +15 m s^{-1} at $r = 10$ km. Most of this spinup is due to the eddy vorticity flux. The fact that the summation of the horizontal terms in the momentum budget agrees very well
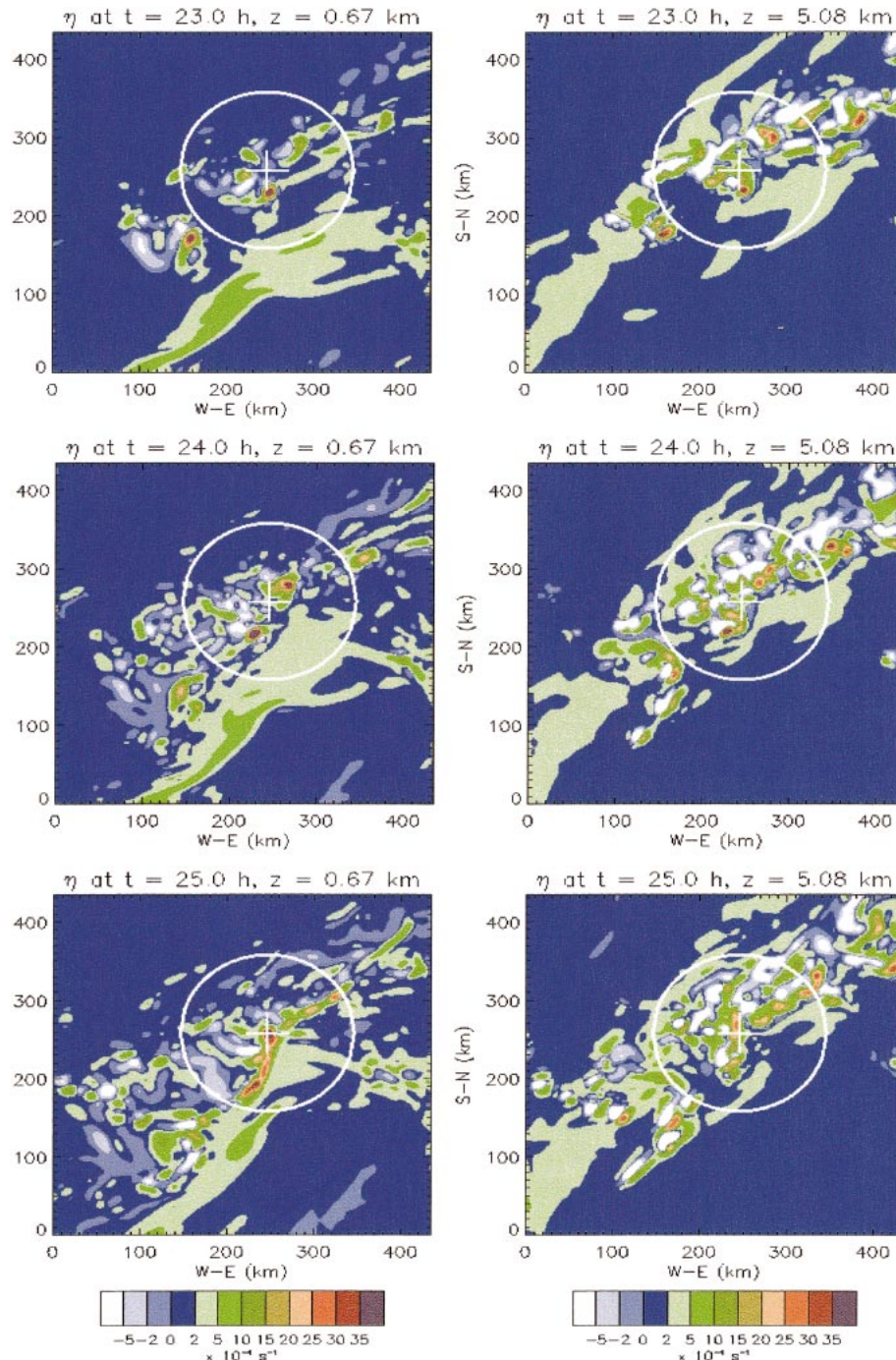
FIG. 7. Plan views of absolute vertical vorticity at low and middle levels of the troposphere during budget A. Fixed center is denoted by the cross, and the budget domain is inside the white circle.

with the actual spinup, suggests that this event is strongly analogous to barotropic dynamics, but with the additional feature of a mean radial inflow generated by diabatic processes. This event is also a strong vortex merger, particularly below $z = 3$ km.

The heat budget of this event (Fig. 13) shows that significant warming occurs. Peak warming of 5 K occurs at midlevels in the core region, and there is a broad area of warming within $r \leq 20$ km from the event center (Fig. 13b). In this event, there exists a very localized pocket of subsidence warming (shown by the strong contour gradient near $r = 0$ km, $z = 3$ km in Fig. 13d).
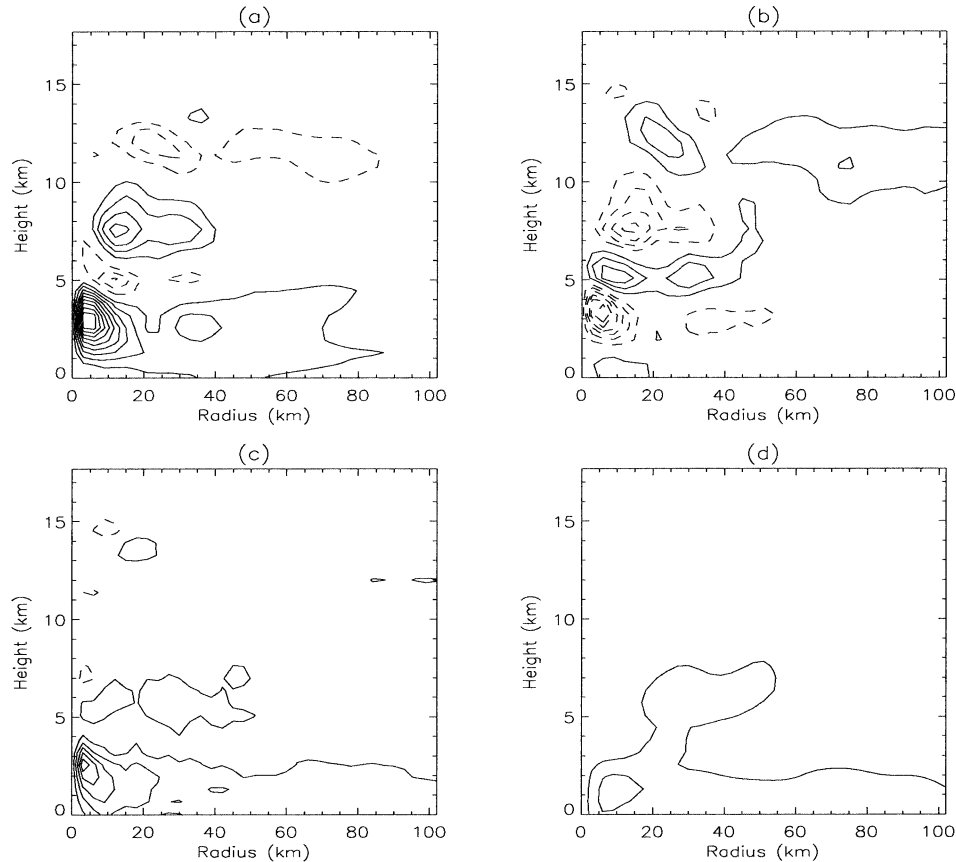
FIG. 8. Integrated local tangential momentum budget for event A in the radius–height domain. Acceleration tendencies are integrated at 10-min increments from $t = 22$ to $t = 25$ h: (a) $\int_{22}^{25} -\overline{u}\,\overline{\eta}\; dt$ is mean horizontal vorticity flux ; (b) $\int_{22}^{25} -\overline{u'\zeta'}\; dt$ is eddy horizontal vorticity flux; (c) $\int_{22}^{25} -\overline{u}\,\overline{\eta}\; dt -\int_{22}^{25} \overline{u'\zeta'}\; dt$ is total horizontal vorticity flux; (d) actual $\Delta\overline{v}$ observed in MM5 model. Contour interval is 5 m s^{-1}. Negative values are denoted by dashed contours and the zero contour is omitted.

However, the broad regional warming encompassed by the 1-K contour in Fig. 13b is primarily due to the imbalance of the diabatic heating and adiabatic cooling in the convective region.

c. Discussion

Based on the foregoing results, two phase of genesis are elucidated in the 3-km numerical simulation. In the first phase, the lower troposphere is "vortically preconditioned" as the hot towers converge and stretch ambient low-level vorticity into small-scale anomalies (cf. Ooyama 1982). In the second phase, multiple mergers of these lower-tropospheric cyclonic PV anomalies occur. Multiple hot towers are found to pulse in the first phase, with convective lifetimes on the order of an hour or less, competing with one another for available CAPE and angular momentum in order to sustain themselves. The strong updrafts in these towers initially create strong cyclonic vorticity anomalies, and then this vorticity diffuses and weakens as the hot tower dies. There is also a larger-scale low-level net convergence of am-

bient relative angular momentum that causes a net increase in the relative vorticity in the vicinity of the hot towers (see, e.g., Fig. 7, green-colored values). This low-level net convergence is important and evident in the storm-relative tangential momentum budget (Figs. 8a,b); a strong mean spinup is competing with a strong eddy spindown (due to the competing hot towers) near the event center. In the second phase (Fig. 11), the enhanced cyclonic circulation increases the likelihood of tropical storm formation. Via these two evolutionary phases, the small-scale hot towers, in conjunction with the low-level net convergence of relative angular momentum, serve to "cascade" the vertical vorticity from the hot tower scale to the tropical cyclone scale. This upscale growth is depicted in Fig. 14. Here, the azimuthal mean vertical vorticity associated with a typical vortical hot tower at $t = 23$ h (left) is shown in comparison to the emergent tropical storm vortex at $t = 36$ h (right). In going from the hot tower to the tropical storm vortex, the horizontal scale of the relative vorticity quadrupled. The core magnitude decreased
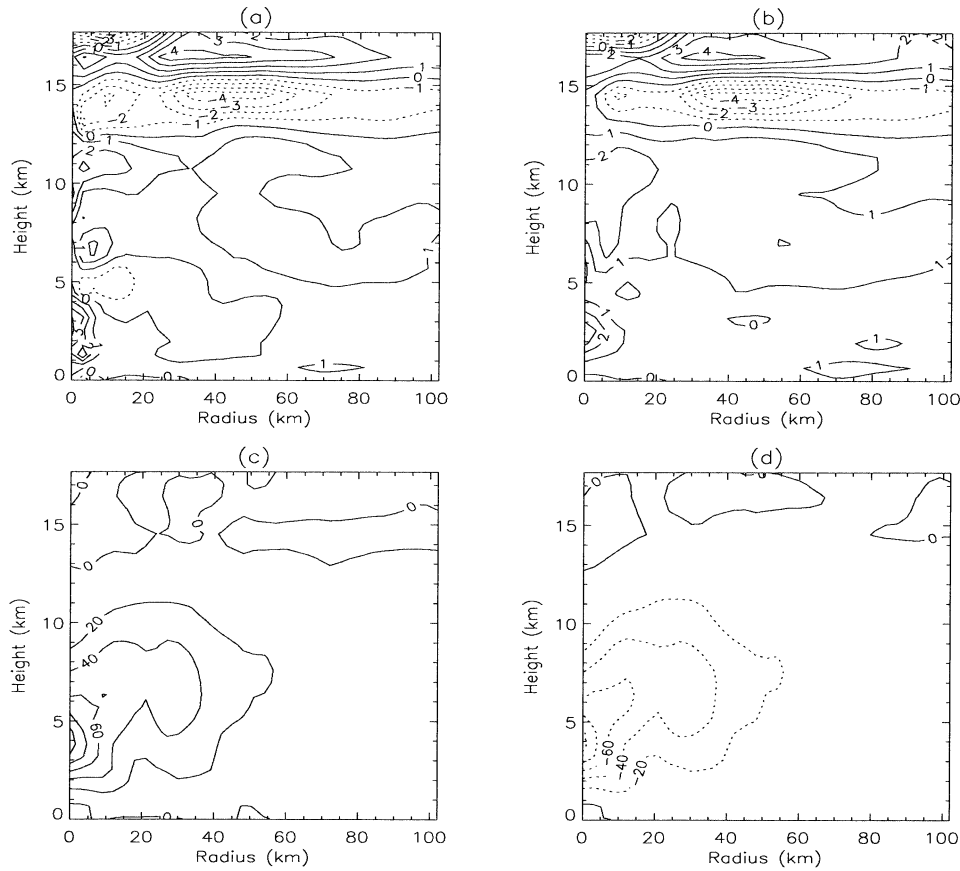
FIG. 9. Integrated local heat budget for event A in the radius–height domain. Heating tendencies are integrated at 10-min increments from $t = 22$ to $t = 25$ h: (a) estimated $\Delta\overline{\theta}$ [summation of terms on right-hand side of (8)]; (b) actual $\Delta\overline{\theta}$ observed in MM5 model; (c) $\int_{22}^{25} \dot{\overline{\theta}}\, dt$; (d) $\int_{22}^{25} -\overline{w}\partial\overline{\theta}/\partial z\, dt$. Contour intervals for (a) and (b) are 1 K, and contour intervals for (c) and (d) are 20 K. Negative values are denoted by dashed contours.

slightly in this transition, from $\overline{\zeta}_{max} \approx 40 \times 10^{-4}$ s^{-1} to $\overline{\zeta}_{max} \approx 30 \times 10^{-4}$ s^{-1}.

5. Quasi-balanced evolution?

The hot towers and the environment in which they form have been shown to be highly vortical. Because of this, we anticipate that less heat energy will be dispersed to the environment via gravity waves than in a nonrotating hot tower. In effect, the heat becomes locally trapped in the vicinity of the rotating convective cores. This is similar to the "heat trapping" concept elucidated by Schubert and Hack (1982) and Hack and Schubert (1986), who demonstrated that the conversion of heat energy to kinetic energy becomes more efficient with an increase in the inertial stability of the tropical cyclone vortex as a whole. The difference here, however, is that the heat trapping is being invoked on the hot tower scale. Because of the strong vorticity in the hot towers and their environment, we surmise that the balance approximation may be valid locally at many stages of the organizational process and valid more generally on the

macroscale comprising a complex of towers. We now look to explore this with a simple balance model.

a. Eliassen's balanced vortex model

Balance models have proven useful for gaining basic dynamical insight into the behavior of atmospheric motions on many different scales. For example, the simplification of the full primitive equations to quasigeostrophic theory has proved to be invaluable for understanding synoptic-scale motions (e.g., Holton 1992). For geophysical vortices, Eliassen's balanced vortex model (Eliassen 1951) is a useful starting point for understanding the axisymmetric behavior of a balanced vortex in the presence of local heat and momentum sources. We wish to understand the degree in which the genesis of the tropical cyclone proceeds in quasi balance. For simplicity, we adopt a version of Eliassen's balanced vortex model in pseudoheight coordinates (Hoskins and Bretherton 1972) in the limiting case of the Bousinessq approximation (e.g., Shapiro and Willoughby 1982):
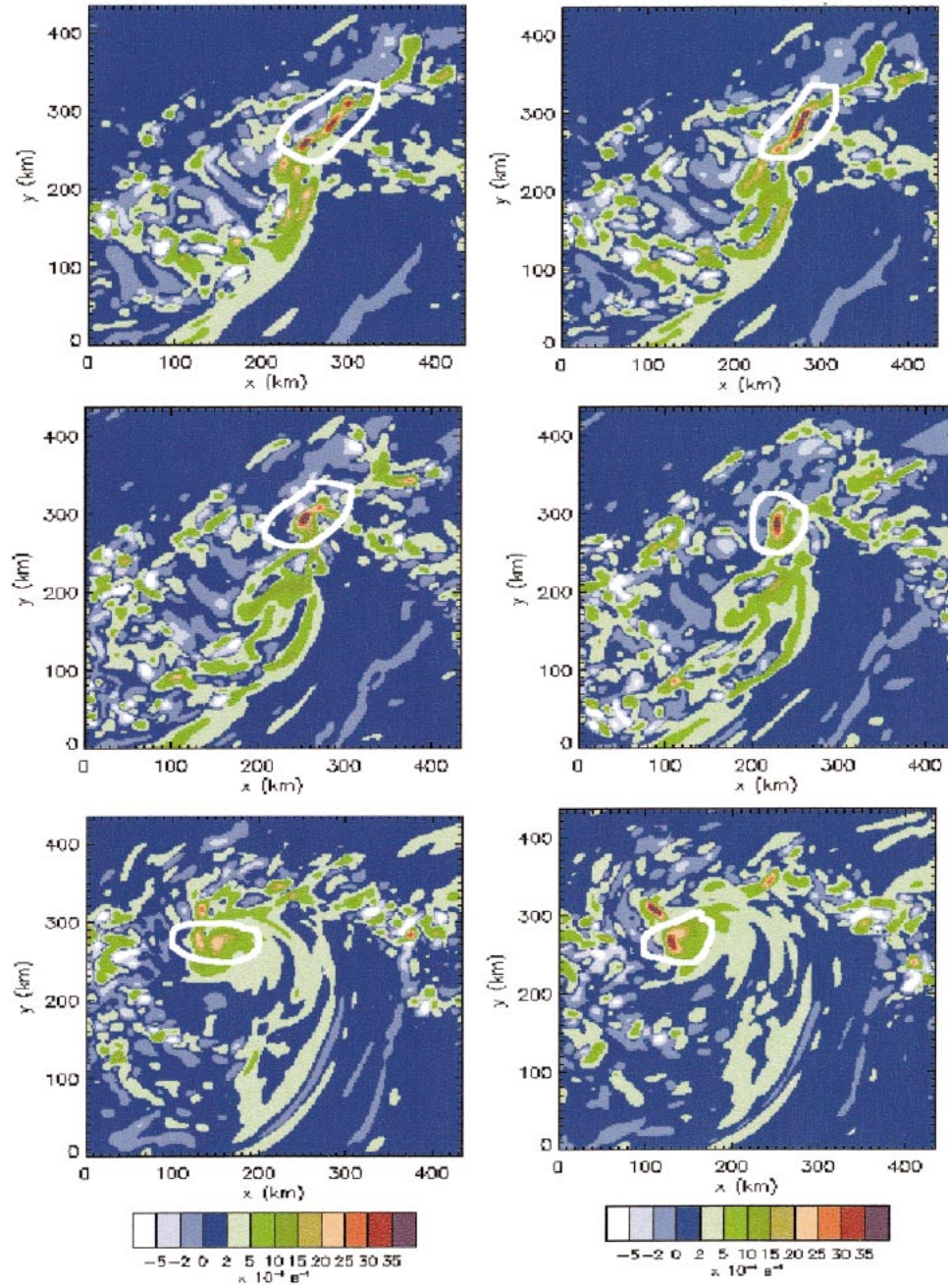
FIG. 10. Three examples of diabatic vortex mergers that occur in the second developmental phase in the genesis of Diana are depicted with each row representing the (left) ''before'' and (right) ''after'' stage of the diabatic vortex merger. In each, absolute vertical vorticity is plotted at $z = 0.67$ km in the entire 3-km domain (similar to Figs. 7 and 11) and each ''before–after'' sequence is approximately $t = 0.5$ h apart. The diabatic vortex mergers are highlighted by white circles. Times are (first row) $t = 26$ h, (second row) $t = 27$ h, and (third row) $t = 33$ h.

$$\frac{\partial}{\partial r}\left(\frac{N^2}{r}\frac{\partial\overline{\psi}}{\partial r} - \frac{\overline{\xi}}{r}\frac{\partial\overline{v}}{\partial z}\frac{\partial\overline{\psi}}{\partial z}\right) + \frac{\partial}{\partial z}\left(\frac{\overline{\xi}\,\overline{\eta}}{r}\frac{\partial\overline{\psi}}{\partial z} - \frac{\overline{\xi}}{r}\frac{\partial\overline{v}}{\partial z}\frac{\partial\overline{\psi}}{\partial r}\right)$$

$$= \frac{\partial\overline{Q}}{\partial r} - \frac{\partial}{\partial z}(\overline{\xi}\,\overline{F}). \tag{9}$$

Here, $\overline{\psi}$ is the mean transverse streamfunction from which the mean radial velocity ($\overline{u}$) and vertical velocity ($\overline{w}$) are determined, $\overline{u} = (-1/r)\partial\overline{\psi}/\partial z$ and $\overline{w} = (1/r)\partial\overline{\psi}/\partial r$; $\overline{N}^2 = \partial^2\overline{\Phi}/\partial^2 z$ is the static stability parameter; $\overline{\xi} = f + 2\overline{v}/r$ is twice the local absolute rotation
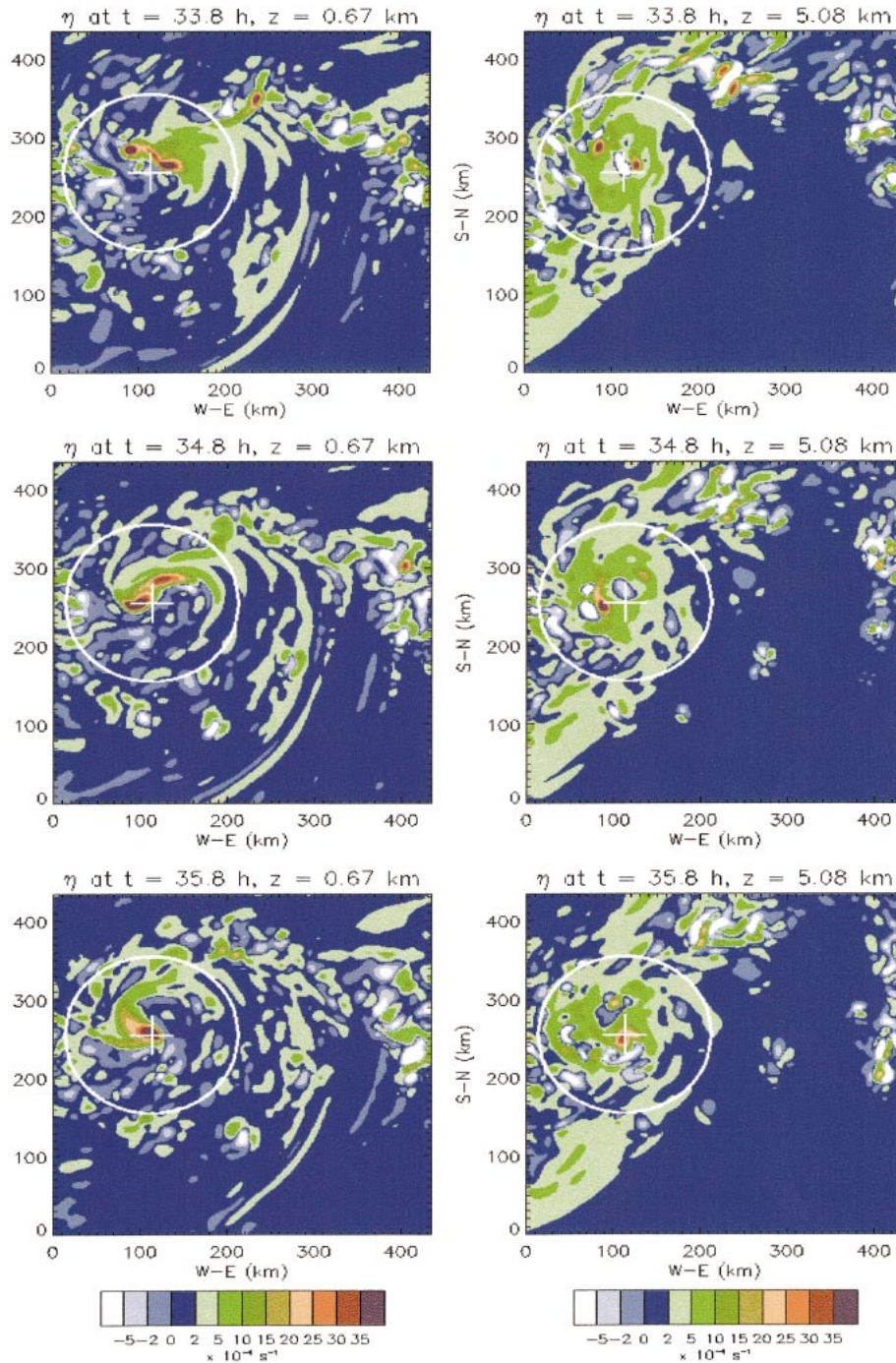
FIG. 11. Plan views of absolute vertical vorticity at low and midlevels of the troposphere during budget B. Fixed center is denoted by the cross, and the budget domain is inside the white circle.

rate of a fluid element at radius r (hereafter the vortex inertia parameter); $\overline{v}$ is the azimuthal mean tangential velocity; $\overline{\eta}$ is the azimuthal mean absolute vertical vorticity at radius r; and $\overline{Q}$ and $\overline{F}$ are the azimuthal mean thermodynamic and momentum forcings introduced into the balance model. The forcings $\overline{F}$ and $\overline{Q}$ are defined as follows:

$$\overline{F} = -\overline{u'\zeta'} - \overline{w'\frac{\partial v'}{\partial z}} + \overline{PBL} + \overline{DIFF}, \quad (10)$$

$$\overline{Q} = \frac{g}{\theta_0}\left(-\overline{u'\frac{\partial \theta'}{\partial r}} - \overline{w'\frac{\partial \theta'}{\partial z}} + \overline{\dot{\theta}}\right). \quad (11)$$

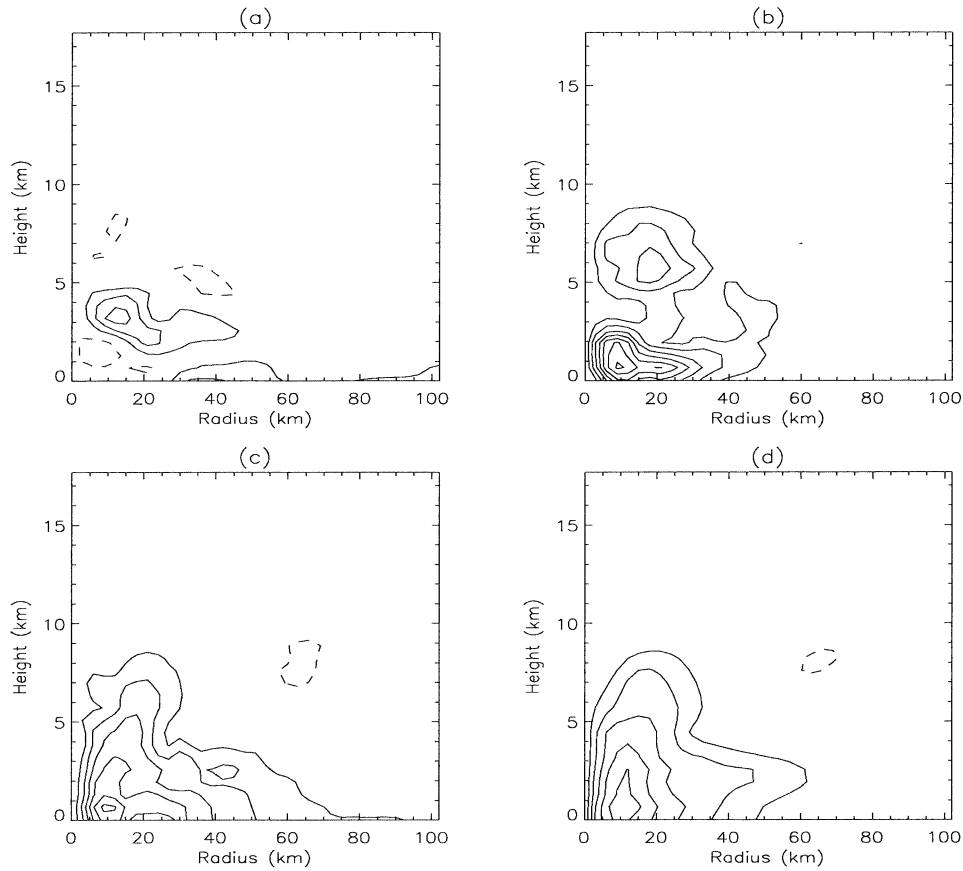Recall that PBL represents the model planetary

FIG. 12. Integrated local tangential momentum budget for event B in the radius–height domain. Acceleration tendencies are integrated at 10-min increments from $t = 33.0$ to $t = 35.8$ h: (a) $\int_{33.0}^{35.8} -\overline{u}\,\overline{\eta}\ dt$ is mean horizontal vorticity flux; (b) $\int_{33.0}^{35.8} -\overline{u'\eta'}\ dt$ is eddy horizontal vorticity flux; (c) $\int_{33.0}^{35.8} -\overline{u}\,\overline{\eta}\ dt - \int_{33.0}^{35.8} \overline{u'\zeta'}\ dt$ is total horizontal vorticity flux; (d) actual $\Delta\overline{v}$ observed in MM5 model. Contour interval is 3 m s^{-1}. Negative values are denoted by dashed contours and the zero contour is omitted.

boundary layer subgrid-scale scheme and DIFF represents the model horizontal diffusion (see sections 2 and 4a for details).

The Sawyer–Eliassen equation is a second-order partial differential equation for the transverse streamfunction forced by local azimuthal mean diabatic heating and friction terms, as well as by eddy fluxes of heat and momentum. The Sawyer–Eliassen equation is an elliptic partial differential equation, and the vortex is gravitationally and symmetrically stable as long as the discriminant is positive. For a Boussinesq fluid in pseudoheight coordinates, the discriminant is defined below (Shapiro and Montgomery 1993):

$$\underbrace{\overline{N}^2\overline{\eta}\,\overline{\xi} - \left(\overline{\xi}\frac{\partial\overline{v}}{\partial z}\right)^2}_{\text{discriminant}} > 0. \qquad (12)$$

The discriminant is calculated with the MM5 data and during the genesis phase is generally found to be positive in the middle and lower troposphere. As an example of this, the discriminant, along with the three

stability parameters of $\overline{N}^2$, $\overline{\eta}$, and $\overline{\xi}$, are shown in Fig. 15 in the local radius–height domain at $t = 34.5$ h about the center marked by the white cross in Fig. 11. In the top left of Fig. 15, it is clear that the discriminant is positive throughout the middle and lower troposphere of the radius–height domain. The absolute vertical vorticity and inertia parameter (top right and bottom right) are generally positive at low and middle levels and negative at upper levels. Here, the static stability ($\overline{N}^2$) is also positive in the entire domain, indicating that the evolution is constrained to proceed under gravitational stability.

At times (such as in Fig. 15), there are found to be very localized pockets (typically at upper levels) where small negative discriminant values exist. When the discriminant has negative values in portions of the radius–height domain, we solve the Sawyer–Eliassen model in two manners via successive overrelaxation (SOR; e.g., Press et al. 1992): (i) not adjusting the negative discriminant values, and (ii) relaxing the negative values to positive values (following the regularization procedure described in Möller and Shapiro 2002). Solutions
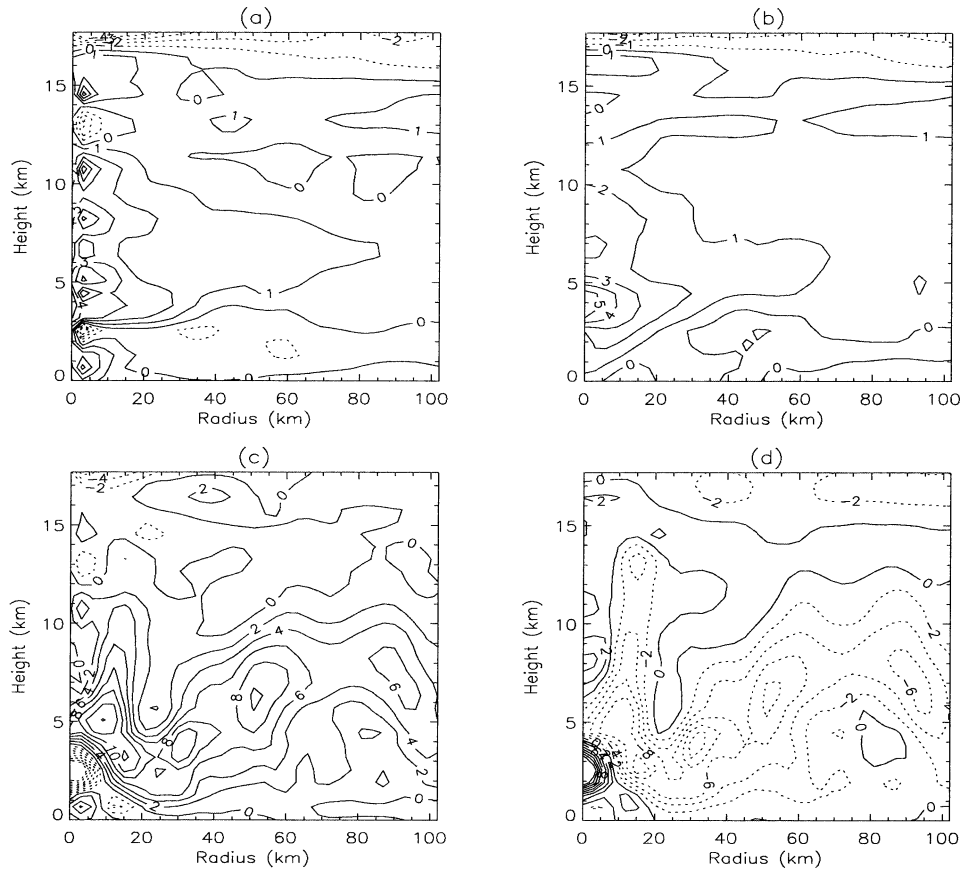
FIG. 13. Integrated local heat budget for event B in the radius–height domain. Heating tendencies are integrated at 10-min increments from $t = 33.0$ to $t = 35.8$ h: (a) estimated $\Delta \overline{\theta}$ [summation of terms on right-hand side of (8)]; (b) actual $\Delta \overline{\theta}$ observed in MM5; (c) $\int_{33.0}^{35.8} \dot{\overline{\theta}} \, dt$; (d) $\int_{33.0}^{35.8} -\overline{w} \partial \theta / \partial z \, dt$. Contour intervals for (a) and (b) are 1 K, and contour intervals for (c) and (d) are 2 K. Negative values are denoted by dashed contours.

for both methods are found to be very similar, indicating that these weak localized pockets of negative discrimant values do not adversely affect the global solution. The use of an overrelaxation technique, rather than a direct solver, allows the larger-scale solution to remain intact in the presence of locally negative discriminant values. In the results presented here the discriminant is not adjusted. This is in fact more realistic since we are not artificially modifying the MM5 model data. The two events documented in section 4 are now examined with this model with the centers shown in Figs. 7 and 11, respectively.

b. MM5 versus Sawyer–Eliassen comparison

The solution of the Sawyer–Eliassen equation is depicted in the local radius–height domain in Figs. 16 and 17. In Fig. 16, the solution is shown at a characteristic time during event A ($t = 24$ h), and in Fig. 17 the solution is shown at a characteristic time during event B ($t = 35.5$ h). In each figure the azimuthal mean secondary circulation of the MM5 simulation is compared

to the mean secondary circulation of the Sawyer–Eliassen model. These are instantaneous comparisons and there is no time averaging of the data. At $t = 24$ h, the solution is depicted through a smaller-scale convective complex of hot towers, and at $t = 35.5$ h the solution is depicted through the nascent tropical cyclone vortex (see Fig. 11). The solution to the Sawyer–Eliassen model is output on the same grid as the analyzed MM5 data ($\Delta r = 3$ km, $\Delta z \approx 600$ m).

The Sawyer–Eliassen mean secondary circulation compares well with the MM5 mean secondary circulation in each of these events, as shown by the figures. In Fig. 16, at $t = 24$ h, the MM5 mean secondary circulation through a convective complex (associated with a PV anomaly cluster) is depicted. There is generally strong inflow at low levels (below $z = 4$ km) and outflow at mid- to upper levels (above $z = 5$ km), and rising motion through the convective region. The balanced secondary circulation diagnosed from the Sawyer–Eliassen model broadly compares well to the MM5 mean secondary circulation, qualitatively and quantitatively. The same comparison is depicted at a later time
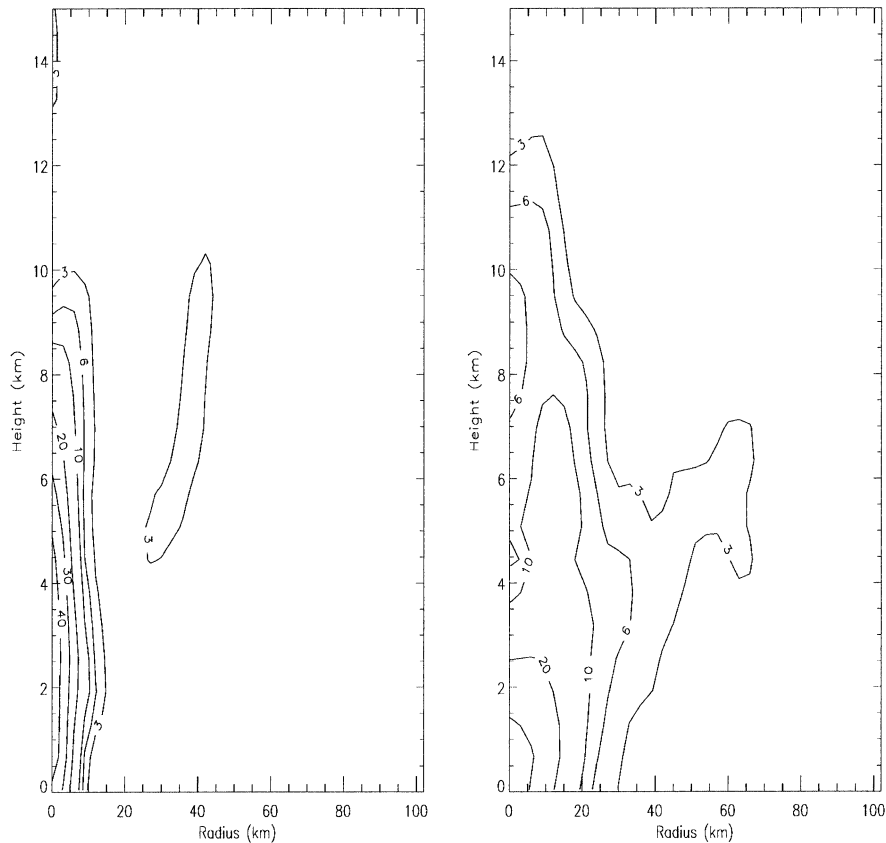
F_{IG}. 14. Azimuthal mean relative vorticity for (left) a single vortical hot tower at $t = 23$ h and (right) for the tropical storm vortex at $t = 36$ h in the local radius–height domain. The contours depicted are $(3, 6, 10, 20, 30, 40) \times 10^{-4}$ s^{-1}.

during event B (Fig. 17) when Diana has a well-defined closed circulation and is near tropical storm strength. In each case, the Eliassen model broadly captures the local mean secondary circulation of the MM5 model. It is noteworthy to see that the Eliassen model captures the subsidence in the vortex core (bottom two panels of Fig. 17, cf. Fig. 13). Numerous other events were examined at many other different times and a similar good comparison was observed.

Since the Sawyer–Eliassen/MM5 comparison is good, it stands to reason that the simulated genesis around event centers is proceeding via approximate gradient and hydrostatic balance in the coarse-grained sense of the azimuthal mean. An examination of the stability parameters required in the Eliassen model shows that static stability and the discriminant are generally positive almost everywhere in the domain (Fig. 15). These are necessary conditions for quasi balance. A further condition is that the flow be rotationally dominant in the sense that the relative verticity vorticity (ζ) is large compared to the horizontal divergence (δ) (McWilliams 1985; Davis and Emanuel 1991). That is, in Cartesian coordinates,

$$|\zeta| = \left| \frac{\partial v}{\partial x} - \frac{\partial u}{\partial y} \right| \gg \left| \frac{\partial u}{\partial x} + \frac{\partial v}{\partial y} \right| = |\delta|.$$

As an illustration, the absolute vertical vorticity and horizontal divergence in the lower troposphere are compared during typical times in the evolution, and the results are displayed at $t = 34.0$ h in Fig. 18. The maximum low-level vorticity exceeds 60×10^{-4} s^{-1} while the maximum convergence is approximately 15×10^{-4} s^{-1}.

6. A simple comparison of moist and dry vortex merger

In previous sections we have demonstrated that, in the cloud-resolving numerical simulation, Hurricane Diana was built by the vortical hot towers in two phases: (i) preconditioning and (ii) multiple vortex mergers and axisymmetrization of small-scale cyclonic PV anomalies. In specific events in each of these phases, we have shown that the spinup of tangential momentum is due primarily to the horizontal vorticity flux, that is, $\overline{u}\,\overline{\eta} + \overline{u'\zeta'}$ (Figs. 8 and 12). The vertical momentum transport
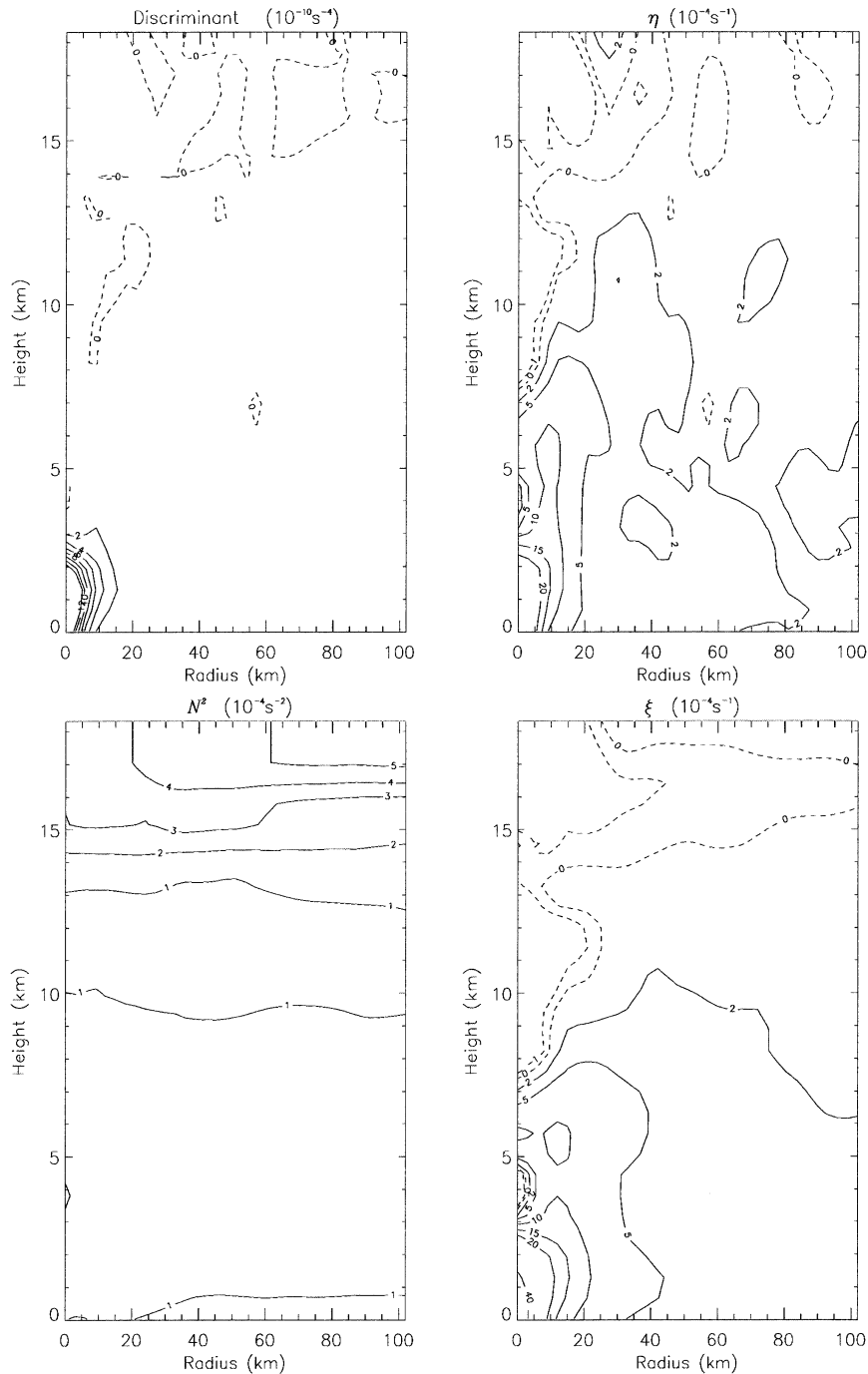
FIG. 15. Azimuthal mean depiction of Eliassen stability parameters in the radius–height domain at $t = 34.5$ h about the center marked by the white cross in Fig. 11. (top left) Discriminant, (top right) static stability, (bottom left) absolute vertical vorticity, and the (bottom right) vortex inertia parameter. Zero and negative values are denoted by dashed contours.

terms are generally found to be quite small in comparison. These results suggest that potentially a large portion of the dynamics occurring here may be explained by quasibarotropic dynamics.

a. Shallow water primitive equation model

To test this hypothesis, a characteristic merger event is examined in a barotropic model, specifically the shal-
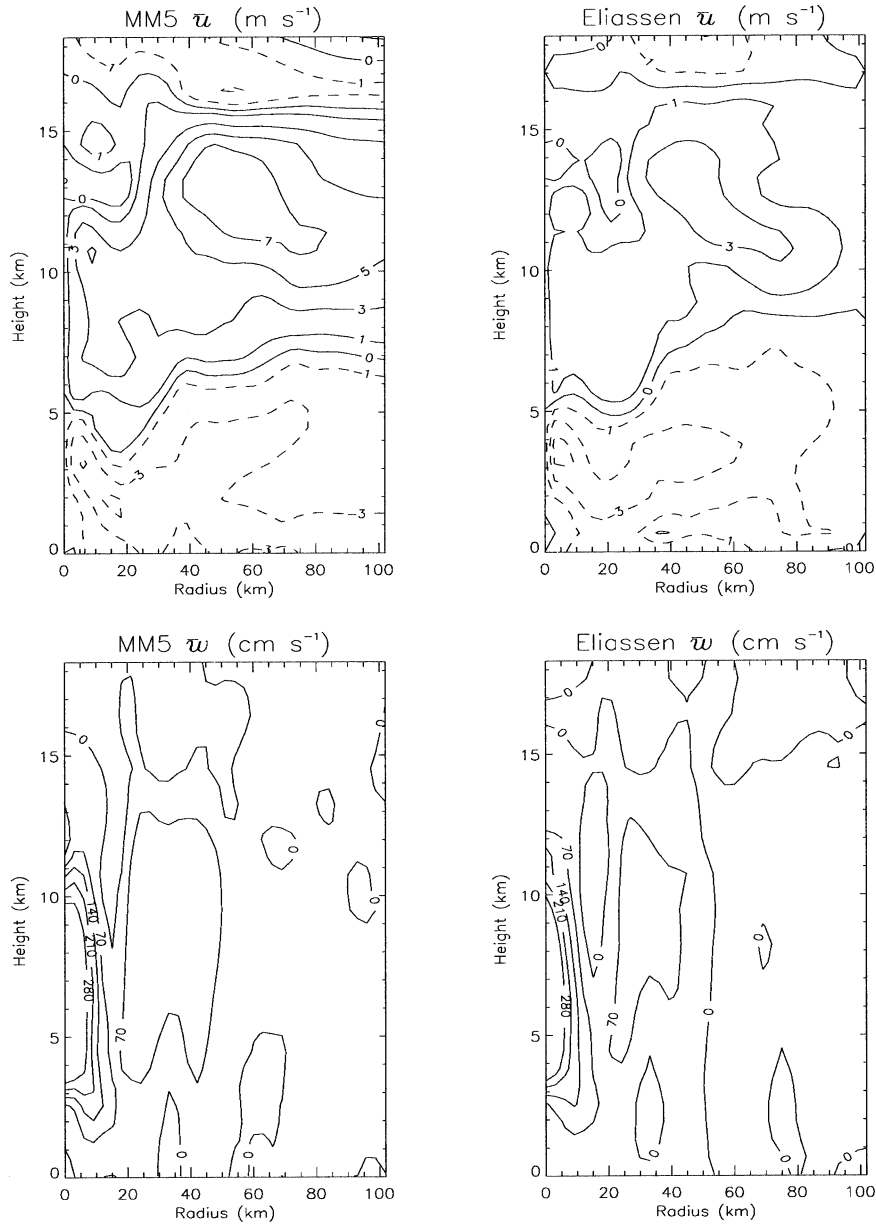
FIG. 16. MM5 simulation mean secondary circulation vs Sawyer–Eliassen balanced mean secondary circulation at $t = 24$ h. The mean radial velocity is shown in the top, and the mean vertical velocity in shown in the bottom. Contour intervals for the mean radial velocity are -7, -5, -3, -1, 0, 1, 3, 5, 7 m s^{-1}, and contour intervals for the mean vertical velocity are -280, -210, -140, -70, 0, 70, 140, 210, 280 cm s^{-1}. Negative contours are dashed.

low water primitive equation (SWPE) model. The model prognostic equations used here are defined on an f plane:

$$\frac{\partial u}{\partial t} - \eta V + \frac{\partial H}{\partial x} + \nu_4 \nabla^4 u + \beta(u - \overline{u}_0) = 0, \quad (13)$$

$$\frac{\partial v}{\partial t} + \eta U + \frac{\partial H}{\partial y} + \nu_4 \nabla^4 v + \beta(v - \overline{v}_0) = 0, \quad (14)$$

$$\frac{\partial P}{\partial t} + \frac{\partial U}{\partial x}\frac{\partial V}{\partial y} + \nu_4 \nabla^4 P + \beta(P - \overline{P}_0) = 0. \quad (15)$$

Here, u is the zonal velocity, v is the meridional velocity, $P = gh$ is the geopotential, g is the acceleration due to gravity, h is the fluid depth, $U = Pu$ and $V = Pv$ are the depth-integrated horizontal momenta, $H = P + 1/2(u^2 + v^2)$ is the Bernoulli function, and $\eta = (\partial v/\partial x - \partial u/\partial y + f)/P$ is here the potential
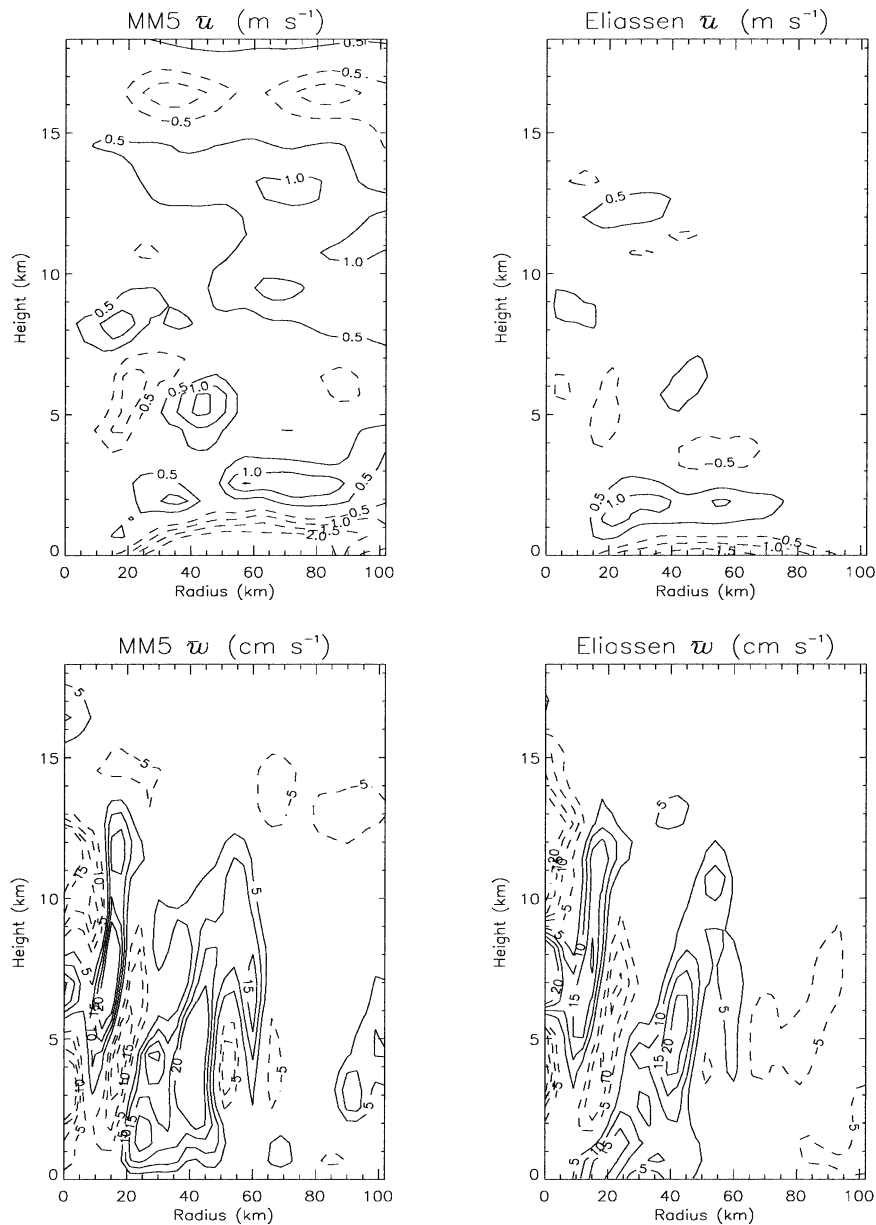
FIG. 17. MM5 simulation mean secondary circulation vs Sawyer–Eliassen balanced mean secondary circulation at $t = 35.5$ h. The mean radial velocity is shown in the top, and the mean vertical velocity in shown in the bottom. Contour intervals for the mean radial velocity are -2, -1.5, -1, -0.5, 0.5, 1, 1.5, 2 m s^{-1}, and contour intervals for the mean vertical velocity are -20, -15, -10, -5, 5, 10, 15, 20 cm s^{-1}. Negative contours are dashed.

vorticity. The β terms are Rayleigh friction terms localized in a sponge layer at large radius to prevent the reflection of gravity waves excited in the vortical region either by initial imbalances or spontaneous radiation in the ensuing vortex dynamics. The initial-state values are denoted by u_0, v_0, and P_0. A fourth-order Runge–Kutta scheme is used for the integration of the SWPE model. The model includes a fourth-order hyperdiffusion of u, v, and P to remove small-scale effects associated with the enstrophy cascade. Potential

vorticity and enstrophy are conserved to a high degree in this model. More detail on the specifics of this shallow water model can be found in Sadourney (1975) and Enagonio and Montgomery (2001).

b. Vortex merger comparison

As discussed in section 4, a major merger of two intense vortex tubes occurs around $t = 34.0$ h in the MM5 simulation. This merger is characterized by a
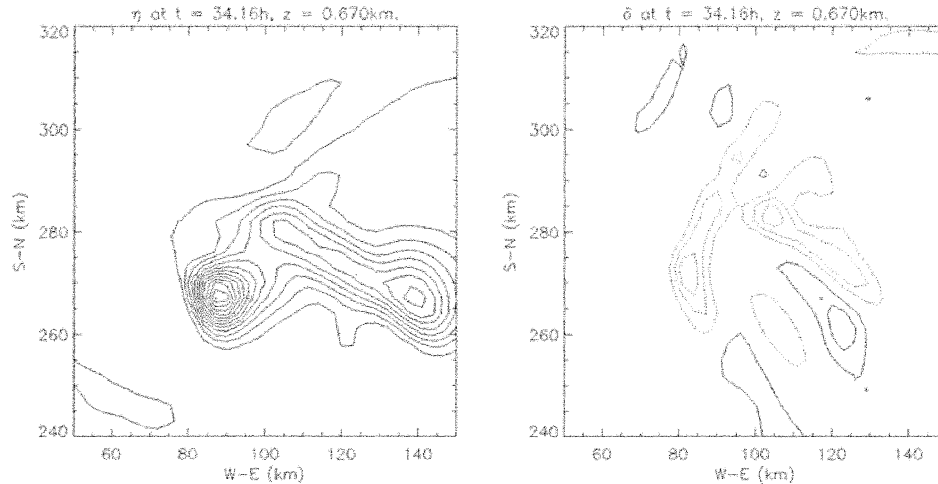
FIG. 18. Absolute vertical vorticity and horizontal divergence at $t = 34.2$ h, $z = 0.67$ km. Contour interval is 5×10^{-4} s^{-1}.

strong spinup in tangential momentum and warming at low levels. The spinup of tangential momentum was shown to be dominated by the horizontal momentum fluxes. The SWPE model is used to analyze the barotropic aspects of this event. The model is initialized with the MM5 horizontal wind data at $z = 0.67$ km, $t = 33.8$ h and the initial fluid (layer) depth is set at $h_0 = 1$ km. The model is configured with a domain of 146×146 grid points spaced 3 km apart in the x and y directions for a total domain size of 438 km $\times$ 438 km, exactly the same configuration as domain 4 in the MM5 simulation. The SWPE model is initialized with two coherent low-level vortices, which are loosely connected (note, $t = 0$ corresponds to the initialization state for the beginning of the vortex merger event, or at approximately $t = 33.8$ h in the MM5 simulation).

A side-by-side summary of the results of SWPE/MM5 comparison is displayed in Fig. 19. Merger does occur in the SWPE model; however, it takes approximately twice as long as in the MM5 model. Although the resultant vorticity anomaly from the SWPE model is weaker and in a different location than the MM5 simulation, we believe the results are nevertheless physically meaningful. First, since merger occurs in both model simulations, this event has strong analogs to barotropic dynamics (McWilliams 1984), as hypothesized. Second, the fact that the SWPE model yields a merger that takes approximately twice as long as in the MM5 model suggests that a net convergence can *accelerate* the merger process in the real atmosphere. The latter conclusion is broadly consistent with numerical simulations of the binary interaction of full-fledged hurricane vortices (Wang and Holland 1995). The emphasis here, however, is on the merger/axisymmetrization dynamics of the much smaller horizontal-scale hot tower vortices. Based on these results, further work examining the physics of three-dimensional vortex tube mergers in the moist atmosphere appears warranted.

7. Conclusions

The role of vortical hot towers in tropical cyclogenesis is to our knowledge examined for the first time in the framework of a three-dimensional full-physics near-cloud-resolving mesoscale model numerical simulation. Our principal finding is that the most important influence to the cyclogenesis of Hurricane Diana are small-scale cores of deep cumulonimbus convection that form in a vorticity-rich environment. A two-phase evolution driven by the vortical hot towers is suggested in the numerical simulation: (i) "vorticity" preconditioning of the lower troposphere via the generation of multiple small-scale intense cyclonic vortex tubes (cf. Ooyama 1982), and (ii) multiple mergers/axisymmetrization of these tubes in the lower troposphere (e.g., McWilliams 1984; Melander et al. 1988; ME98; Möller and Montgomery 2000; Enagonio and Montgomery 2001).

Although the "diabatic" mergers/axisymmetrization of the tubes is the primary mechanism by which the local-scale tangential momentum spinup and warm-core formation occurs, here, the low-level influx of mean angular momentum (driven by the diabatic heating of the ensemble of hot towers) is equally important for increasing the macroscale low-level vertical vorticity and tangential winds throughout the genesis (see also Montgomery et al. 2004, manuscript submitted to *J. Atmos. Sci.*). As a noteworthy example of vortex merger, a peak low-level tangential wind spinup of 15 m s^{-1} and peak warming of 5 K is achieved over a 3-h time frame in a characteristic event examined. Compressional warming by subsidence is not found here to be a primary mechanism for warm-core development. Rather, latent heat released by the deep cumulonimbus convection tends to be trapped by the strong vorticity in the hot towers, and the warm core there is built in the same manner as the local tangential momentum spinup; via
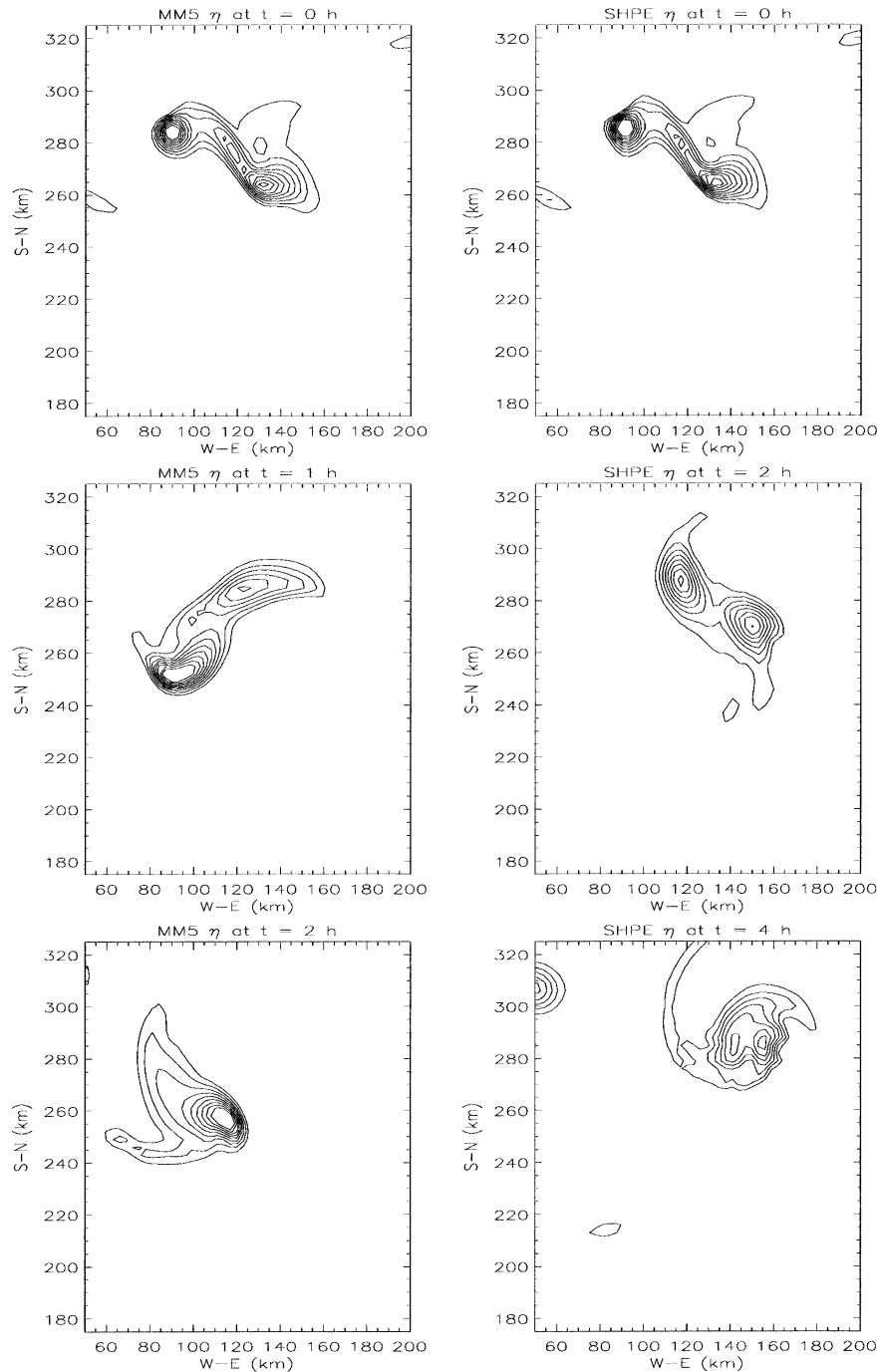
FIG. 19. Side-by-side comparison of the absolute vertical vorticity evolution at $z = 0.67$ km in the MM5 and shallow water primitive equation (SWPE) models. The initialization time ($t = 0$) corresponds to $t = 33.8$ h in the MM5 simulation, or near the beginning of the vortex merger event B summarized in Fig. 10. Contour intervals are 0.001, 0.0015, 0.002, 0.003, 0.0035, 0.004, 0.0045, 0.005 s^{-1}.

diabatic mergers/axisymmetrization of small-scale lower-tropospheric cyclonic vorticity tubes.

Simpler models are examined to elucidate the underlying dynamics of tropical cyclogenesis as simulated here. Using the Sawyer–Eliassen balanced vortex model, the cyclogenesis of Diana is demonstrated to proceed in approximate gradient and hydrostatic balance in the vicinity of vortex structures, or a quasi-balanced evolution where radial and vertical accelerations are small. The strong vorticity and gravitational stability of the

local environment and the convection is the primary reason for the quasi-balanced evolution. Since vortex merger appears to be a crucial mechanism for genesis in this case, the dynamics of vortex merger in the simulated moist atmosphere are examined more closely. The diabatic vortex mergers seen in the MM5 simulation are roughly captured by a dry barotropic shallow water model. Since low-level merger occurs approximately one-half as fast in the dry barotropic model in a characteristic event, we infer, consistent with Wang and Holland (1995), that moist convective effects and attending secondary circulations *accelerate* the low-level merger process in the real atmosphere and tend to produce a merged vortex that is significantly stronger than its dry-merged counterpart. Further work examining the dynamics of three-dimensional diabatic vortex mergers appears warranted.

In summary, we have demonstrated an upscale growth mechanism for tropical cyclogenesis where small-scale vortical hot towers are the building blocks. As is well known, a necessary condition for cyclone formation is for the spinup tendency by a net convergence of absolute angular momentum to exceed the spindown effect associated with surface friction (e.g., Raymond et al. 1998). This simulation demonstrates that this net convergence may be produced by numerous small-scale areas of deep convection rather than a broad larger-scale area of net convergence. We believe the high-resolution simulation employed here provides new and useful insights into the internal mechanisms leading to tropical cyclogenesis given favorable environmental conditions already exist. The Diana case confirms the importance of low-level diabatic vortex merger and vortex axisymmetrization processes associated with deep convective episodes (ME98; Möller and Montgomery 2000; Enagonio and Montgomery 2001). Whether the formation process in the deep Tropics proceeds along similar lines with the vortical hot towers playing an essential role in the organizational process is an open question. Further three-dimensional modeling studies using idealized flow configurations are currently underway and are advocated to obtain a more complete understanding of the upscale growth process suggested here.

Based on the foregoing results, we recommend the following.

- Increase emphasis on documenting the life cycle of vortical hot towers, including their attendant vorticity and PV signatures, during the formation of tropical cyclones. Cloud-resolving numerical models in idealized configurations should be used for this purpose so as to isolate the basic dynamics of and interactions between these important structures in prehurricane environments.
- Increase emphasis on quantifying how fragile the formation process is to adverse affects, such as enhanced vertical shear or depleted moisture. We also advocate the comparison of both cloud-resolving and opera-

tional models in realistic adverse environments so as to identify the reasons for "false alarms," a known weakness of many operational models.
- Emphasize obtaining in situ data of sufficient spatial and temporal resolution during the tropical cyclone formation period, including both flight-level data and airborne Doppler radar data. Given the fact that vortical hot tower lifetimes in this numerical simulation are on the order of 1 h, we advocate data sampling at a minimum temporal resolution of 30 min and spatial resolution of 3 km. These data are essential to assess the realism of high-resolution near-cloud-resolving simulations, such as the Diana case decribed in this manuscript.
- Emphasize obtaining a comprehensive understanding of vortical hot towers. Specifically, what controls the development and areal density of rotating hot towers? How does rotation affect the dynamics of the hot towers? How does rotation affect the production of downdrafts?

REFERENCES

Ayotte, B. A., and H. J. S. Fernando, 1994: The motion of a turbulent thermal in the presence of background rotation. *J. Atmos. Sci.,* **51,** 1989–1994.
Bister, M., and K. Emanuel, 1997: The genesis of Hurricane Guillermo: TEXMEX analyses and a modeling study. *Mon. Wea. Rev.,* **125,** 2662–2682.
Bosart, L. F., and J. Bartlo, 1991: Tropical storm formation in a baroclinic environment. *Mon. Wea. Rev.,* **119,** 1979–2013.
Charney, J. G., and A. Eliassen, 1964: On the growth of the hurricane depression. *J. Atmos. Sci.,* **21,** 68–75.
Cotton, W. R., and R. A. Anthes, 1989: *Storm and Cloud Dynamics.* Academic Press, 883 pp.
Davis, C. A., and K. Emanuel, 1991: Potential vorticity diagnostics of cyclogenesis. *Mon. Wea. Rev.,* **119,** 1929–1953.
——, and L. Bosart, 2001: Numerical simulations of the genesis of Hurricane Diana (1984). Part I: Control simulation. *Mon. Wea. Rev.,* **129,** 1859–1881.
——, and ——, 2002: Numerical simulations of the genesis of Hurricane Diana (1984). Part II: Sensitivity of track and intensity prediction. *Mon. Wea. Rev.,* **130,** 1100–1124.
Dudhia, J., 1989: Numerical study of convection observed during the Winter Monsoon Experiment using a mesoscale two-dimensional model. *J. Atmos. Sci.,* **46,** 3077–3107.
——, 1993: A nonhydrostatic version of the Penn State–NCAR me-

soscale model: Validation tests and simulation of an Atlantic cyclone and cold front. *Mon. Wea. Rev.,* **121,** 1493–1513.

Eliassen, A., 1951: Slow thermally or frictionally controlled meridional circulation in a circular vortex. *Astrophys. Norv.,* **5,** 18–60.

Enagonio, J., and M. T. Montgomery, 2001: Tropical cyclogenesis via convectively forced vortex Rossby waves in a shallow water primitive equation model. *J. Atmos. Sci.,* **58,** 685–706.

Gray, W. M., 1968: Global view of the origins of tropical disturbances and storms. *Mon. Wea. Rev.,* **96,** 669–700.

Grell, G. A., J. Dudhia, and D. R. Stauffer, 1995: A description of the fifth-generation Penn State/NCEP mesoscale model (MM5). NCAR Tech. Note NCAR/TN-398+STR, 122 pp.

Hack, J. J., and W. H. Schubert, 1986: Nonlinear response of atmospheric vortices to heating by organized cumulus convection. *J. Atmos. Sci.,* **43,** 1559–1573.

Helfrich, K. R., 1994: Thermals with background rotation and stratification. *J. Fluid Mech.,* **259,** 265–280.

Holton, J. R., 1992: *An Introduction to Dynamic Meteorology.* Academic Press, 511 pp.

Hong, S.-Y., and H.-L. Pan, 1996: Nocturnal boundary layer vertical diffusion in a medium-range forecast model. *Mon. Wea. Rev.,* **124,** 2322–2339.

Hoskins, B. J., and F. P. Bretherton, 1972: Atmospheric frontogenesis models: Mathematical formulation and solution. *J. Atmos. Sci.,* **29,** 11–36.

——, M. E. McIntyre, and A. W. Robertson, 1985: On the use and significance of isentropic potential vorticity maps. *Quart. J. Roy. Meteor. Soc.,* **111,** 877–946.

Julien, K., S. Legg, J. McWilliams, and J. Werne, 1996: Rapidly rotating turbulent Rayleigh–Benard convection. *J. Fluid Mech.,* **322,** 243–273.

——, ——, ——, and ——, 1999: Plumes in rotating convection. Part 1. Ensemble statistics and dynamical balances. *J. Fluid Mech.,* **391,** 151–187.

Kain, J. S., and J. Fritsch, 1990: A one-dimensional entraining/detraining plume model and its application in convective parameterization. *J. Atmos. Sci.,* **47,** 2784–2802.

Legg, S., K. Julien, J. McWilliams, and J. Werne, 2001: Vertical transport by convective plumes. *Phys. Chem. Earth,* **26B,** 259–262.

McWilliams, J. C., 1984: The emergence of isolated coherent vortices in turbulent flow. *J. Fluid Mech.,* **146,** 21–43.

——, 1985: A uniformly valid model spanning the regimes of geostrophic and isotropic, stratified turbulence: Balanced turbulence. *J. Atmos. Sci.,* **42,** 1773–1774.

Melander, M. V., N. Zabusky, and J. McWilliams, 1988: Symmetric vortex merger in two dimensions: Causes and conditions. *J. Fluid Mech.,* **195,** 303–340.

Möller, J. D., and M. T. Montgomery, 2000: Tropical cyclone evolution via potential vorticity anomalies in a three-dimensional balanced model. *J. Atmos. Sci.,* **57,** 3366–3387.

——, and J. Shapiro, 2002: Balanced contributions to the intensification of Hurricane Opal as diagnosed from a GFDL model forecast. *Mon. Wea. Rev.,* **130,** 1866–1881.

Montgomery, M. T., and B. Farrell, 1993: Tropical cyclone formation. *J. Atmos. Sci.,* **50,** 285–310.

——, and J. Enagonio, 1998: Tropical cyclogenesis via convectively forced vortex Rossby waves in a three-dimensional quasigeostrophic model. *J. Atmos. Sci.,* **55,** 3176–3207.

Ooyama, K., 1964: A dynamical model for the study of tropical cyclone development. *Geofis. Int.,* **4,** 187–198.

——, 1969: Numerical simulation of the life cycle of tropical cyclones. *J. Atmos. Sci.,* **26,** 3–40.

——, 1982: Conceptual evolution of the theory and modeling of the tropical cyclone. *J. Meteor. Soc. Japan,* **60,** 369–379.

Powers, J. G., and C. Davis, 2002: A cloud resolving regional simulation of tropical cyclone formation. *Atmos. Sci. Lett.,* **3,** 15–24.

Press, W. H., S. Teukolsky, W. Vetterling, and B. Flannery, 1992: *Numerical Recipes in Fortran 77. The Art of Scientific Computing.* 2d ed. Cambridge University Press, 933 pp.

Raymond, D. J., C. López-Carrillo, and L. L. Cavazos, 1998: Case studies of developing East Pacific easterly waves. *Quart. J. Roy. Meteor. Soc.,* **124,** 2005–2034.

Riehl, H., and J. Malkus, 1958: On the heat balance in the equatorial trough zone. *Geophysica,* **6,** 503–538.

Ritchie, E. A., and G. Holland, 1997: Scale interaction during the formation of Typhoon Irving. *Mon. Wea. Rev.,* **125,** 1377–1396.

Rotunno, R., and K. Emanuel, 1987: An air–sea interaction theory for tropical cyclones. Part II: Evolutionary study using a nonhydrostatic axisymmetric numerical model. *J. Atmos. Sci.,* **44,** 542–561.

Sadourney, R., 1975: The dynamics of finite-difference models of the shallow-water equations. *J. Atmos Sci.,* **32,** 680–689.

Schubert, W. H., and J. J. Hack, 1982: Inertial stability and tropical cyclone development. *J. Atmos. Sci.,* **39,** 1687–1697.

Schultz, P., 1995: An explicit cloud physics parameterization for operational numerical weather prediction. *Mon. Wea. Rev.,* **123,** 3331–3343.

Shapiro, L. J., and H. Willoughby, 1982: The response of balanced hurricanes to local sources of heat and momentum. *J. Atmos. Sci.,* **39,** 378–394.

——, and M. Montgomery, 1993: A three-dimensional balance theory for rapidly rotating vortices. *J. Atmos. Sci.,* **50,** 3322–3335.

Simpson, J., J. B. Halverson, B. S. Ferrier, W. A. Petersen, R. H. Simpson, R. Blakeslee, and S. L. Durden, 1998: On the role of "Hot Towers" in tropical cyclone formation. *Meteor. Atmos. Phys.,* **67,** 15–35.

Wang, Y., and G. Holland, 1995: On the interaction of tropical-cyclone-scale vortices. IV: Baroclinic vortices. *Quart. J. Roy. Meteor. Soc.,* **121,** 95–126.